BOSTON UNIVERSITY

y Master Thesis entitle
tial Flow Around Liftin
1974, by Edward A. Ch

al Continuum
ollege of Engineering
5

DEPARTMENT OF AEROSPACE AND MECHANICAL ENGINEERING

BOSTON UNIVERSITY

COLLEGE OF ENGINEERING

STEADY INCOMPRESSIBLE POTENTIAL FLOW AROUND LIFTING BODIES IMMERSED IN A FLUID

by

Edward A. Chiuchiolo

B.S.A.E., BOSTON UNIVERSITY

(1970)

Submitted in partial fulfillment

of the requirements for the

degree of Master of Science

in Aerospace Engineering

1974

APPROVED BY

Chairman _____
Associate Professor of Aerospace Engineering

First Reader _____
Professor of Aerospace Engineering

Second Reader _____
Associate Professor of Systems Engineering

FOREWORD

This work was partially supported by NASA Grant NGR 22-004-030. Dr. E. Carson Yates, Jr., acted as Technical Advisor for the Grant.

ACKNOWLEDGEMENTS

I would like to express my sincere appreciation to Dr. Luigi Morino for the advice, assistance and patience he has given me during the development of this thesis. His contributions have been invaluable. Also, I thank Dr. Daniel Udelson and Dr. P. T. Hsu for their interest and comments. Finally, I thank my typist and literary editor, my wife Janice, for her patience and thoughtfulness.

ABSTRACT

The objective of this thesis is the refinement of a method for evaluating the pressure distribution on a body surface of arbitrary shape in incompressible flow.

The solution to the problem is obtained in terms of the velocity potential. However, the formulation for the potential cannot be solved in closed form with the exception of a few special cases. Hence, the solution must be obtained through numerical approximations which require the use of a high speed digital computer.

Two different numerical formulations are considered here. In the first method, the box method, the body surface is approximated by N small elements, Σ . Within these elements or boxes, the value of the potential, φ , is considered constant and equal to the value at the center of the element, φ_i . This results in a system of N linear, algebraic equations in N unknowns.

The other method is the collocation method in which the unknown function is approximated by a linear combination of N prescribed functions which satisfy the boundary conditions of the problem and N unknown coefficients resulting in a system of linear, algebraic equations. The specific approach applied here is called the modal method.

In this thesis, both of these methods are applied to a very thin, rectangular wing in incompressible, steady flow. Of the two methods,

the box method is more practical as it is applicable to more general geometries (the modal method requires a new set of functions for each geometry) and requires less computer time (fifty percent of that required by the modal method for the same problem).

CONTENTS

CONTENTS CONTINUED

LIST OF FIGURES

LIST OF SYMBOLS

a	speed of sound
$[A_{ki}]$	$[D_{ki}] - [C_{ki}] - [W_{ki}]$
b	span
b_k	coefficient of source distribution
B_k	$[A_{ki}]^T \left\{ b_i \right\}$
c	chord
c_{kj}	coefficient of doublet distribution
C_{kj}	coefficient of doublet distribution in modal method
C_p	coefficient of pressure
C_n	coefficient of x modes in modal method
D_m	coefficient of y modes in modal method
D_{kj}	$U_i (P_k)$
E_{mn}	minimum of the sum of the errors for the modal potential equation when satisfied in the least square sense
E_{ki}	$\iint U_i(P_k) \frac{\partial}{\partial n} \left(\frac{1}{r_k} \right) d\Sigma$
h	thickness ratio, i.e., ratio of maximum body thickness to chord
h_{max}	maximum thickness ratio
I_D	integral of doublets
I_S	integral of sources
I_W	wake contribution integral

J	wake coefficient
NX	number of wing boxes in X direction
NY	number of wing boxes in Y direction
$\hat{N}$	$2 \cdot NX \cdot NY$
P	pressure
$[Q_{kj}]$	$[A_{ki}]^T [A_{ij}]$
$U_j(P)$	potential mode shape function
x,y,z	body control points
x_1,y_1,z_1	dummy integration points
x_*,y_*,z_*	limit as body approaches body surface
$\Delta x, \Delta y$	grid mesh size
Φ	velocity potential
φ	perturbation potential
Φ_j	unknown coefficients in modal method, $f(x,y)$
φ^s	symmetric perturbation potential
ξ,η	rectangular wing coordinates
τ	wing thickness, percent of chord
δ_{kj}	Kroneker delta
Ψ,Θ	intermediate coordinate transformations
ρ	$(\xi_i^2+\eta_i^2)^{1/2}$
$\Delta\psi$	difference in potential on wake
Ω	solid angle representation of wake
α,β	constants in tangent plane method
Σ	body surface

W	wake contribution

SUBSCRIPTS

p	plus
m	minus
l	dummy point of integration
*	point of evaluation
W	wake contribution
ℓ	index along trailing edge boxes

SUPERSCRIPTS

c	center
—	coordinates in nonuniform box definition

1. THEORETICAL FORMULATION

1.1 Introduction

The problem of evaluating the pressure distribution on a wing immersed in a fluid has, in the past, and is presently attracting a great deal of attention. The most common method applied is that of lifting surface theories using the velocity potential. The principal equation used is an integral equation which relates the pressure-difference distribution over the body surface with the downwash produced by the body surface. This integral equation may be expressed as[1]:

$$\omega(x,y)=\frac{1}{4\rho U_\infty}\iint_S \Delta p(\xi,\eta)\,K(x,\xi,y,\eta,M)\,d\xi\,d\eta \qquad 1.1$$

where the pressure difference, Δp, is the unknown, and $K(x,\xi,y,\eta,M)$ is the so-called Kernel function.

There are two major objections to this type of approach. The first of these is that the numerical solution of this equation is quite complicated. The difficulties arise from the rather complicated Kernel function and the numerical integration of improper integrals. The second objection is that lifting-surface theories are not easily generalized to include more complicated geometries. Similar objections hold for the problem of oscillating wings. An excellent analysis of the status of art is given in Ref. 2.

In order to circumvent these problems, a general method has been developed in Ref. 3. This method is valid for both compressible and incompressible potential flows around bodies of arbitrary shape in arbitrary motion. The formulation is based on Green's formula for the equation of unsteady compressible potential aerodynamic flow. Although theoretical formulation given in Ref. 3 is very general, the application of the method is limited to thin wings in steady subsonic flow. The objective of this thesis is to explore further the applicability of the method mentioned above. However, this analysis is limited, for simplicity, to steady, incompressible flow. In the rest of this section, the method developed in Ref. 3 is summarized for the particular case of steady, incompressible flow.

1.2 Statement of the Problem

The equation for steady incompressible potential aerodynamic flow is given by the well known Laplace's equation[1]

$$\nabla^2 \phi = 0 \tag{1.2}$$

where ϕ is the velocity potential. Let the surface of the body, Σ be given by the equation

$$S_B(x,y,z) = 0 \tag{1.3}$$

Then the tangency boundary conditions are given by[1]

$$\frac{\partial \phi}{\partial n} = \vec{n} \cdot \nabla \phi = 0 \tag{1.4}$$

where $\vec{n}$ is the normal to the surface Σ. Finally the boundary condition at ∞ is given by

$$\phi = U_\infty x \tag{1.5}$$

By introducing the perturbation potential, φ, such that

$$\phi = U_\infty (x + \varphi) \tag{1.6}$$

equations 1.2, 1.4, and 1.5 yield Eqs. 1.7, 1.8, and 1.9 respectively which are given as:

$$\nabla^2 \varphi = 0 \tag{1.7}$$

and

$$\frac{\partial \phi}{\partial n} = -\frac{1}{|\nabla S_B|} \frac{\partial S_B}{\partial x} \tag{1.8}$$

on the surface Σ_B, and finally

$$\varphi = 0 \tag{1.9}$$

at infinity. The problem is to determine the solution of Eq. 1.7 using the boundary conditions given by Eqs. 1.8 and 1.9. Finally the pressure coefficient may be obtained from the linearized Bernoulli Theorem as[1]

$$P - P_\infty = -\rho_\infty U_\infty^2 \frac{\partial \varphi}{\partial x} \tag{1.10}$$

and the pressure coefficient is given by

$$C_p = \frac{P - P_\infty}{\frac{1}{2}\rho_\infty U_\infty^2} = -2\frac{\partial \varphi}{\partial x} \tag{1.11}$$

1.3 Formulation of the Problem

The basis for the formulation of the problem is Green's formula for the Laplace equation. Green's formula can be expressed as[1]

$$\begin{aligned} \varphi(x,y,z) = &-\iint \frac{\partial \varphi}{\partial n_1}(x_1,y_1,z_1)\,\frac{1}{4\pi r}\,d\Sigma \\ &+ \iint \varphi(x_1,y_1,z_1)\,\frac{\partial}{\partial n_1}\left(\frac{1}{4\pi r}\right) d\Sigma \end{aligned} \tag{1.12}$$

with

$$r = \left[(x-x_1)^2 + (y-y_1)^2 + (z-z_1)^2 \right]^{\frac{1}{2}} \qquad 1.13$$

where (x, y, z) is the control point and (x_1, y_1, z_1) is the dummy point of integration on the surface Σ. The surface Σ surrounds the body and the wake.

From Eq. 1.13 it can be seen that the potential is given by an integral representation composed of sources, $1/4\pi r$, of intensity $(\partial\varphi/\partial n)$ and of doublets, $\partial/\partial n\,(1/4\pi r)$, of intensity φ. The values of $\partial\varphi/\partial n$ are known from the boundary conditions as shown by Fig. 1. All that remains to be determined is the value of φ which is unknown on the body surface.

In order to evaluate φ on the surface Σ let the control point approach a point on the surface Σ. As shown in Appendix A this yields

$$\varphi(x,y,z) = -\iint_{\Sigma} \frac{\partial\varphi}{\partial n}(x_1,y_1,z_1)\,\frac{1}{2\pi r}\,d\Sigma + \iint_{\Sigma} \varphi(x_1,y_1,z_1)\,\frac{\partial}{\partial n_1}\left(\frac{1}{2\pi r}\right) d\Sigma \qquad 1.14$$

Note that Eq. 1.14 differs from Eq. 1.13 by the factor $1/2\pi$ instead of $1/4\pi$. In addition the control point (x, y, z) is on the surface instead of outside. If $\partial\varphi/\partial n$ is known everywhere on Σ, Eq. 1.14 is a Freedholm integral equation of second kind, whose solution exists and is unique (exterior Von Newman's problem of Laplace's equation[3]). However, the surface Σ surrounds not only the body but also the wake. The procedure for treating the contribution of the wake is discussed in the next Subsection, where the integral equation given by Eq. 1.15 is obtained and the methods of solution are outlined in Subsection 1.5.

1.4 The Wake Contribution

As mentioned above, the surface Σ in Eq. 1.14 is composed of two branches; the first, Σ_B, surrounds the body and the second, Σ_W, surrounds the wake. The treatment of the wake introduced in Ref. 3 is used here. The wake is assumed to be composed of straight vortex-lines emanating from the trailing edge of the body. Under this assumption. Eq. 1.14 becomes (see Appendix B)

$$\varphi(x,y,z) = -\iint_{\Sigma_B} \frac{\partial\varphi}{\partial n}(x,y,z)\,\frac{1}{2\pi r}\,d\Sigma_B + \iint_{\Sigma_B} \varphi(x,y,z)\,\frac{\partial}{\partial n}\left(\frac{1}{2\pi r}\right) d\Sigma_B + I_W \qquad 1.15$$

with the wake integral, I_W, given by

$$I_w = \iint_{\Sigma_w} (\varphi_u - \varphi_l) \frac{\partial}{\partial n} \left(\frac{1}{2\pi r}\right) d\Sigma \qquad 1.16$$

where Σ_w is the upper side of the surface of the wake. In the problem considered in the following, the trailing edge is on the plane Z = 0 and thus Eq. 1.16 reduces to

$$I_w = \int_{-b/2}^{+b/2} \Delta\varphi \, J_w \, dy_1$$

where b is the span of the wing and J_w is given by

$$J_w = \frac{Z}{(Y-Y_1)^2 + Z^2} \left[1 - \frac{X_{TE} - X}{\left\{(X_{TE}-X)^2 + (Y_1-Y)^2 + Z^2\right\}^{1/2}} \right]$$

Note that the wake formulation is based on bodies having sharp trailing edge otherwise it is not possible to know where the wake leaves the body.

1.5 Methods of Solution

The necessary relation for evaluation $\mathcal{Q}$ on the body surface is given in Subsection 1.4 as shown in Eq. 1.15. It may be noted that, with the exception of a few special cases, it cannot be solved in closed form. Hence the solution must be obtained through numerical approximate methods, which generally require the use of a high speed digital computer.

Several methods can be used. The one used in Ref. 3, which will be called box method, is summarized here. The surface Σ_B is divided into N small elements (boxes) Σ_i. The value of $\mathcal{Q}$ is assumed to be constant within each element and equal to the value $\mathcal{Q}_i$ at the center of the element. By satisfying Eq. 1.15 at the centers of the elements Σ_i, one obtains a system of N linear algebraic equations with N unknowns, $\mathcal{Q}_i$, which can be easily solved on a computer. A more detailed description of the box method is given in Section 2.

However, one of the most successful methods for lifting surface theories is the collocation method in which the unknown function is approximated by a linear combination of N prescribed functions with N unknown coefficients. The prescribed functions satisfy the boundary conditions of the problem whose N unknown coefficients are determined by solving at N given points (collocation points). Thus before proceeding into a more elaborated problem, the legitimate question of which of the two methods is more convenient for this problem must be

answered. A method equivalent to the collocation method (called modal method) is described in Section 3. The advantage to this method is that it gives a smooth curve solution rather than a solution at discrete points. However, it is limited in that it requires a different set of functions for each particular geometry with increasing difficulty in guessing appropriate functions with more complex geometries, e.g., wing-body interference. Also, this method requires large amounts of computer time, nearly twice the amount required by the other methods explored.

Thus it was decided to continue the analysis of the problem by using the box method. Next it should be noted that in Ref. 3 the coefficient of the equations of the box method are evaluated analytically by assuming that each surface element can be replaced by its tangent plane at the center of the element. This hypothesis is adequate for very thin wings (thickness ratio $\tau \leq 1\%$). However, even for moderately thick wings ($\tau = 10\%$) the condition that, in each equation, the sum of the coefficients be equal to one is only poorly satisfied[3]. Thus another legitimate question must be answered: can the convergence of the solution be improved by using the correct surface element and evaluating the coefficients numerically (instead of analytically)? This method is described in detail in Section 4. The results obtained in Section 6, however, indicate that the condition that in each equation the sum of the coefficients be equal one is fairly well satisfied for thick wings, but poorly satisfied for thin wings.

Hence, a third approach for the evaluation of the coefficients was explored. The coefficients are first evaluated analytically with the tangent plane hypothesis. Then they are corrected by adding the integral of the difference (between correct-element integrand and tangent-plane integrand) evaluated numerically. The details of this procedure are given in Section 5. The results (Section 6) indicate that this procedure (numerical-analytic evaluation of coefficients) is better than the purely analytic and the purely numerical procedure. A diagram outlining the development of the above methods is given in Fig. 2.

2. THE BOX METHOD

2.1 Geometry of the Problem

The body used for studying the relative efficiency of the different methods is the same as that used in Ref. 3, i.e., a rectangular, thin wing in steady flow. For this particular problem, alternate numerical solutions (lifting surface theory, Ref. 4) as well as experimental results (Ref. 5) are available.

The wing used has a symmetric profile with thickness h given by

$$h = \tau c \frac{3\sqrt{3}}{2} \sqrt{\bar{\xi}} (1 - \bar{\xi}) \sqrt{1 - \bar{\eta}^2} \qquad 2.1$$

The thickness ratio (i.e., the ratio of the maximum body thickness to the chord) is given by

$$\tau = \frac{h_{max}}{c} = \frac{h}{c}\Bigg|_{\substack{\bar{\xi} = \frac{1}{3} \\ \bar{\eta} = 0}} \qquad 2.2$$

Rearranging Eq. 2.1 gives the geometry of the wing at zero angle of attack in terms of $\bar{\xi}$ and $\bar{\eta}$ as

$$\bar{x} = c\,\bar{\xi}$$

$$\bar{y} = \frac{b}{2}\,\bar{\eta}$$

$$\bar{z} = \pm \tau c\,\frac{3\sqrt{3}}{4}\sqrt{\bar{\xi}}\,(1-\bar{\xi})\sqrt{1-\bar{\eta}^2} \qquad 2.3$$

with $\bar{\xi}$ and $\bar{\eta}$ given by

$$\bar{\xi} = \frac{\bar{x}}{c}$$

$$\bar{\eta} = \frac{2\bar{y}}{b}$$

and plus (minus) is for the upper (lower) side in Eq. 2.6.

For angle of attack, α, different from zero, the following coordinate transformation is used

$$X = \bar{x}\cos\alpha + \bar{z}\sin\alpha$$

$$y = \bar{y} \qquad 2.4$$

$$z = -\bar{x}\sin\alpha + \bar{z}\cos\alpha$$

For purposes of comparison with the methods presented here and other methods, all results are evaluated at an angle of attack of 5° (Fig. 3).

2.2 The Box Method

The box method is used to evaluate the coefficients of the source, doublet and wake contributions. First consider the body surface, Σ_B, as divided into elements $d\Sigma_i$. With this assumption, Eq. 1.15 can be written as

$$2\pi\,\varphi(p) = \iint_{\Sigma_B} \frac{\partial \varphi}{\partial n}\,\frac{1}{r}\,d\Sigma_B + \sum_{i=1}^{N} \iint_{\Sigma_i} \varphi\,\frac{\partial}{\partial n}\left(\frac{1}{r}\right) d\Sigma_i + I_w \qquad 2.5$$

Applying the Mean Value Theorem and assuming that the potential can be approximated by the value at the center of the element yields

$$2\pi\,\varphi(p) = \iint_{\Sigma_B} \frac{\partial \varphi}{\partial n}\,\frac{1}{r}\,d\Sigma_B + \sum_{i=1}^{N} \varphi_i \iint_{i} \frac{\partial}{\partial n}\left(\frac{1}{r}\right) d\Sigma_i + \sum_{l} \varphi_l w_l \qquad 2.6$$

where the index ℓ applies to the trailing edge boxes only for wake considerations. Finally, satisfying Eq. 2.8 at P(k), the centers of the elements yield

$$\varphi_K = b_K + \sum c_{Ki}\, \varphi_i + \sum w_{Ki}\, \varphi_i \qquad 2.7$$

The coefficients b_k, c_{ki}, and w_{ki} are defined by

$$b_K = \iint_{\Sigma_B} \frac{\partial \varphi}{\partial n}\, \frac{1}{r_K}\, d\Sigma_B \qquad 2.8$$

$$c_{Ki} = \iint_{\Sigma_i} \frac{\partial}{\partial n} \left(\frac{1}{r_K}\right) d\Sigma_i \qquad 2.9$$

and

$$w_1 = + \int_{\Delta Y_1} J_1 \, dY_1 \qquad 2.10$$

Rearrangment gives the final form as

$$\sum_i a_{ki} \cdot \varphi_i - b_k = 0 \qquad 2.11$$

with

$$a_{ki} = \delta_{ki} - c_{ki} - w_{ki} \qquad 2.12$$

where δ_{ki} is the usual Kronecker Delta.

2.3 Definition of Boxes

In defining the boxes on the body surface, first consider the classical transformations.

$$X = c\xi \qquad 0 \le \xi \le 1$$
$$Y = \frac{b}{2}\eta \qquad -1 \le \eta \le +1 \qquad 2.13$$

This reduces the wing to one with chord equal to one and span equal to two (Fig. 4). Note that $\partial S / \partial x_1$, and $\partial S / \partial y_1$ are infinite at the leading edge and tip of the wing, respectively. This suggests a modification of the body surface boxes that gives a better description of the leading edge and the tip. This is best accomplished by using a non-uniform mesh for the definition of the boxes which is expressed mathematically by the transformation,

$$\bar{\xi} = \bar{x}^2 \qquad 0 \le \bar{x} \le 1$$
$$\bar{\eta} = \left[1 - (1-\bar{y})^2\right]\frac{\bar{y}}{|\bar{y}|} \qquad -1 \le \bar{y} \le 1 \qquad 2.14$$

This causes the boxes at the leading edge and the tip to be smaller than those not along the leading edge and tip (Fig. 5). Boxes of constant size $\Delta\bar{X}$, $\Delta\bar{Y}$ in the plane $\bar{X}$, $\bar{Y}$ given by

$$\Delta \bar{x} = 1/NX$$
$$\Delta \bar{y} = 1/NY \qquad 2.15$$

are used where NX and NY are the number of boxes in direction $\bar{X}$ and $\bar{Y}$, respectively. In other words, the center of the box, (m, n) is given by (see Fig. 5),

$$\bar{X}_m^{(c)} = (m - \tfrac{1}{2})\Delta\bar{x} \quad m=1,\ldots,NX$$
$$\bar{Y}_m^{(c)} = (n - \tfrac{1}{2})\Delta\bar{y} \quad n=1,\ldots,NY \qquad 2.16$$

whereas, its boundaries are given by,

$$\bar{X}_m^{(m)} \leq \bar{X} \leq \bar{X}_m^{(p)}$$
$$\bar{Y}_n^{(m)} \leq \bar{Y} \leq \bar{Y}_n^{(p)} \qquad 2.17$$

with

$$\bar{x}_m^{(m)} = \bar{x}_m^{(c)} - \frac{\Delta\bar{x}}{2} = (m-1)\,\Delta\bar{x}$$

$$x_m^{(p)} = \bar{x}_m^{(c)} + \frac{\Delta\bar{x}}{2} = m\,\Delta\bar{x}$$

$$\bar{y}_n^{(m)} = \bar{y}_n^{(c)} - \frac{\Delta\bar{y}}{2} = (n-1)\Delta\bar{y} \qquad 2.18$$

$$\bar{y}_n^{(p)} = \bar{y}_n^{(c)} + \frac{\Delta\bar{y}}{2} = n\,\Delta\bar{y}$$

Note that, for each set of values m and n, there are two boxes, one on the upper and one on the lower side of the wing; hence, the total number of boxes on the right hand part of the wing is

$$\hat{N} = 2 \cdot NX \cdot NY \qquad 2.19$$

2.4 Comments

The results obtained in Ref. 3 indicate that the method is both fast and accurate for very small thicknesses. However, the condition

$$\sum_{i=1}^{N} C_{ki} = -1 \qquad 2.20$$

(which should be satisfied by the coefficients C_{ki}, Ref. 3, Eq. 7.22) is satisfied within a 4% tolerance for thickness ratio τ = 1% while for τ = 10%, the condition is only satisfied within a 24% tolerance. In order to improve this condition, two approaches are available: trying a different method or improving the evaluation of the coefficients in the box method. Both approaches are explores in Section 3 and Section 4 respectively.

3. THE MODAL METHOD

3.1 Introduction

The so-called modal method is a method for determining the pressure distribution on a body surface by approximating the shape of the aerodynamic potential with a series of mode shapes in the spanwise and chordwise directions. Once the shape of the potential has been determined, the pressure distribution can be obtained by differentiating according to Eq. 1.11. The results obtained from this method are in very close agreement with those obtained with the box method.

Although a straight forward, fairly uncomplicated method that gives good results in a wide range of thickness ratios, this method has one undesirable quality. It is quite good for relatively simple geometries but assuming the series representation of the potential for more involved geometries is quite difficult. One of the main interests in evaluating the pressure distribution is for wing-body interference and for this method, estimating a potential shape such as this would be quite difficult. Also, this method requires large computer time, up to twice as much as the box method.

3.2 Theory

As mentioned in Section 1, an alternate method, the modal method, is explored before attacking the problem of thick wings. The modal method approach is to approximate the shape of the potential by a series of mode shapes in the chordwise and spanwise directions. This results in a

system of N mode equations with N unknown coefficients. Once the potential distribution has been determined, the pressure distribution can be determined using Eq. 1.11.

The modes of φ are chosen as follows: The function φ can be separated into symmetric and anti-symmetric components with respect to the midplane of the wing (Fig. 6a & b) as,

$$\varphi = \varphi^S + \varphi^A \tag{3.1}$$

The symmetric part is given by (Fig. 6a),

$$\varphi^S = \sum_{1}^{P}\sum_{1}^{Q} \Phi_{pq}\, U^S_{pq}(x,y) \tag{3.2}$$

where

$$U^S_{pq}(x,y) = x^p y^{2q} \tag{3.3}$$

For the anti-symmetric part (Fig. 6b) the modes U^A_{mn} are chosen as follows: consider the classical modal expansion for the pressure coefficient for lifting problems

$$C_p = -2\frac{\partial \varphi}{\partial x} = \sum_{m=0}^{M}\sum_{n=0}^{N} K_{mn}\sqrt{\frac{1-x}{x}}(1-x)^m\sqrt{1-y^2}\,y^{2n} \qquad 3.4$$

which satisfies the Kutta condition at the trailing edge as well as the general behavior shown in Fig. 7. By integration with respect to x, one obtains (Appendix D) a modal expansion for φ given by

$$\varphi = \sum \Phi^A_{mn} U^A_{mn}(x,y) \qquad 3.5$$

where Φ_{mn} is related to K_{mn} by the relation

$$K_{mn} = \Phi^A_{m+1,n}(m+\tfrac{3}{2}) - m\,\Phi^A_{m,n} \qquad m=0,\ldots,M \qquad 3.6$$

(with $\Phi_{M+1} = 0$) and U^A_{mn} are the desired modes for the expansion for φ. The expansion for U^A_{mn} is given by

$$U^A_{mn}(x,y) = \pm \left[-\sqrt{x}\,(1-x)^{m+\frac{1}{2}} + \delta_{m,o} \tan^{-1}\sqrt{\frac{x}{1-x}} \right] \sqrt{1-y^2}\; y^{2n} \qquad 3.7$$

where the plus (minus) sign holds for the upper (lower) surface of the wing and

$$\delta_{m,o} = 1 \quad \text{for} \quad m = 0$$

$$\delta_{m,o} = 0 \quad \text{for} \quad m \neq 0 \qquad 3.8$$

is the well known Kronecker Delta.

Combining Eqs. 3.1, 3.2, and 3.5 one obtains

$$Q = \sum_{1}^{P} \sum_{1}^{Q} \Phi^{S}_{pq} U^{S}_{p,q}(X,Y)$$

$$+ \sum_{1}^{M} \sum_{1}^{N} \Phi^{A}_{mn} U^{S}_{mn}(X,Y) \qquad 3.9$$

Equation 3.9 may be rewritten as

$$Q = \sum_{1}^{PQ+MN} \Phi_{\lambda} U_{\lambda}(X,Y) \qquad 3.10$$

where

$$\Phi_{\lambda} = \Phi^{S}_{pq} \qquad \lambda = 1, \ldots, PQ$$

$$U_{\lambda}(X,Y) = U^{S}_{pq}(X,Y) \qquad \lambda = 1, \ldots, PQ \qquad 3.11$$

with

$$i = p + P(q-1) \qquad 3.12$$

and

$$\Phi_i = \Phi^A_{mn} \qquad i = PQ+1, \ldots, (PQ+MN) \qquad 3.13$$

$$U_i(x,y) = U^A_{mn}(x,y) \qquad i = PQ+1, \ldots, (PQ+MN)$$

with

$$i = PQ + m + M(n-1) \qquad 3.14$$

3.3 Formulation

Consider the equation for the potential on the body surface as given by Eq. 1.16 and repeated here for convenience

$$2\pi\varphi = -\iint_{\Sigma_B} \frac{\partial\varphi}{\partial n}\,\frac{1}{r}\,d\Sigma_B + \iint_{\Sigma_B} \varphi\,\frac{\partial}{\partial n}\left(\frac{1}{r}\right) d\Sigma_B + I\omega \qquad 3.15$$

In the modal method, the unknown φ is assumed to be a linear combination of M known functions, $U_i(P)$, (modes) with M unknown coefficients Φ_i. Mathematically, this is given by Eq. 3.10 or

$$\varphi = \sum \Phi_i\, U_i(P) \qquad 3.16$$

Substitution of Eq. 3.16 into Eq. 3.15 yields

$$2\pi \sum \Phi_i U_i(P) = \iint_{\Sigma_B} \frac{\partial \varphi}{\partial n} \frac{1}{r} d\Sigma_B$$

$$+ \sum \Phi_i \iint_{\Sigma_B} U_i(P) \frac{\partial}{\partial n} \left(\frac{1}{r}\right) d\Sigma_B + I_\omega \qquad 3.17$$

with $\partial\varphi/\partial n$ given by the boundary conditions. Satisfying Eq. 3.17 at M control points P_k yields

$$\sum D_{Ki} \Phi_i = b_K + \sum E_{Ki} \Phi_i \qquad 3.18$$

$$+ \sum W_{Ki} \Phi_i$$

where

$$D_{Ki} = U_i(P_K)$$

$$b_K = \iint_{\Sigma_B} \frac{\partial \varphi}{\partial n} \frac{1}{r_K} d\Sigma_B$$

$$E_{Ki} = \iint_{\Sigma_B} U_i(P_K) \frac{\partial}{\partial n}\left(\frac{1}{r_K}\right) d\Sigma_B \qquad 3.19$$

$$W_{Ki} = \pm \int J_l U_i(P_K) dy_1$$

where J_l is defined in Appendix B and is the wake contribution.

Equation 3.18 can be rewritten as

$$[A_{Ki}]\{\Phi\} = \{b_K\} \qquad 3.20$$

where the matrix A_{ki} is given by

$$[A_{Ki}] = [D_{Ki}] - [E_{Ki}] - [W_{Ki}] \qquad 3.21$$

Once the unknown coefficients Φ_i have been determined, φ can be evaluated from Eq. 3.16. The coefficient b_K can now be evaluated as $\partial\varphi/\partial n$ is known from the boundary conditions. Note that once the values of Φ_i are known, the lifting component of the pressure coefficient can be evaluated using Eq. 3.4 with K_{mn} given by Eq. 3.6.

3.4 Least-Square Modal Method

In the form thus far developed, the modal method can be used but is limited to a small number of collocation points, since for more than a few collocation points computer times are very large (18 minutes is required for 4 collocation points). However, four collocation points does not guarantee that the solution is close to the correct one. For this reason, a method which allows few modes (4 was found to be sufficient) and many collocation points (36 per surface in 18 minutes of computer time) is developed here.

To begin, consider Eq. 3.20 in the following form

$$\sum A_{ij} \Phi_j - b_i = 0 \qquad 3.22$$

If the number of collocation points, or equations (i), is equal to the number of unknowns of modes (j), then Eq. 3.22 can be satisfied exactly. However, for the case when $i > j$, this equation cannot be satisfied exactly, but, rather in the least-square sense. Using the method of least-squares, Eq. 3.22 is replaced by

$$\sum_{i=1}^{N_{Points}} \left(\sum_{j=1}^{M_{modes}} A_{ij} \Phi_j - b_j \right)^2 = \sum_K E_K^2 = E = \min \qquad 3.23$$

where E is the sum of the minimum errors. Note here that $N_{points} \neq M_{modes}$. Next, in order to minimize the error E, set the derivatives of the error with respect to Φ_k equal to zero:

$$\sum_{\lambda} \left\{ 2 \left(\sum A_{\lambda j} \Phi_j - b_\lambda \right) \left[\sum_j \left(\frac{\partial}{\partial \Phi_K} \left(A_{\lambda j} \Phi_j - b_\lambda \right) \right) \right] \right\} = 0 \qquad 3.24$$

Using Eq. 3.26 and expanding Eq. 3.25 yields

$$\sum_{\lambda} \sum A_{\lambda K} A_{\lambda j} \Phi_j - \sum_{\lambda} A_{\lambda K} b_\lambda = 0 \qquad 3.27$$

Since $[A_{ik}] = [A_{ki}]^T$ and rewriting Eq. 3.27 gives

$$[A_{K\lambda}]^T [A_{\lambda j}] \{\Phi_j\} - [A_{K\lambda}]^T \{b_\lambda\} = 0 \qquad 3.28$$

Finally, for convenience, write Eq. 3.28 as

$$[Q_{\kappa j}]\{\Phi_j\} = \{B_\kappa\} \qquad 3.29$$

where

$$[Q_{\kappa j}] = [A_{\kappa i}]^T [A_{\lambda j}]$$

and

$$\{B_\kappa\} = [A_{\kappa i}]^T \{b_i\}$$

4. NUMERICAL EVALUATION OF THE COEFFICIENTS

4.1 Introduction

The purely analytic method, Ref. 3, is limited in that its reliability is not assessed for wings of thickness ratios in excess of 1%. This is true because of the nature of the method but, on the other hand, a purely numerical approach seems well suited to the problem of thick wings. The final results of the purely numerical method shows that although well suited for thick wings, the thicknesses that can effectively be evaluated are too great to be practical. Considering the results of both methods, the reasonable solution is a combination of the two methods, which is considered in Section 5.

4.2 Theory

First consider the surface Σ divided into elements $d\Sigma_i$ as shown in Fig. 8. For this case, Eq. 1.15 is rewritten as

$$2\pi\varphi(P) = \oint\!\!\!\!\!\!\int_{\Sigma_B} \frac{\partial \varphi}{\partial n}\,\frac{1}{r}\,d\Sigma_B + \sum_{i=1}^{N} \iint_{\Sigma_i} \varphi\,\frac{\partial}{\partial n}\left(\frac{1}{r_K}\right) d\Sigma_i + I_W \qquad 4.1$$

where I_W is the contribution of the wake as discussed in Appendix B. The mean value theorem gives

$$\iint_{\Sigma_i} \varphi \frac{\partial}{\partial n}\left(\frac{1}{r}\right) d\Sigma_i = \bar{\varphi}_i \iint_{\Sigma_i} \frac{\partial}{\partial n}\left(\frac{1}{r}\right) d\Sigma_i \qquad 4.2$$

where $\bar{\varphi}_i$ is the appropriate value in the element Σ_i. In other words, $\bar{\varphi}_i$ can be approximated by the value of φ_i at the center of the box. With this in mind, Eq. 4.1 can be written as

$$2\pi\varphi(P) = \iint_{\Sigma_B} \frac{\partial \varphi}{\partial n} \frac{1}{r} d\Sigma_B + \sum_{i=1}^{N} \varphi_i \iint_{\Sigma_i} \frac{\partial}{\partial n}\left(\frac{1}{r}\right) d\Sigma + \sum_{l} \varphi_l w_l \qquad 4.3$$

The l in the last term covers only the trailing edge for the contribution of the wake with

$$w_l = \pm \int_{\Delta y_l} J_l \, dy_1 \qquad 4.4$$

where the plus (minus) sign is used for the upper (lower) side of the wake and J_W is as defined in Appendix B. Finally, by satisfying this equation at P(k), the center of the box, one obtains

$$\varphi_K = b_K + \sum c_{K\lambda}\,\varphi_\lambda + \sum w_{K\lambda}\,\varphi_\lambda \qquad 4.5$$

where

$$b_K = \iint_{\Sigma_B} \frac{\partial \varphi}{\partial n}\,\frac{1}{r}\,d\Sigma_B \qquad 4.6$$

and

$$c_{K\lambda} = \iint_{\Sigma_\lambda} \frac{\partial}{\partial n}\left(\frac{1}{r_K}\right) d\Sigma_\lambda \qquad 4.7$$

The value of r_k is the distance from the dummy point of integration to the center of the element or

$$r_K = (r)\Big|_{P=P(K)} = |P(K) - P_1| \qquad 4.8$$

Finally W_{ki} is given by

$$W_{Ki} = [W_i]\Big|_{P=P(K)} \qquad 4.9$$

for the boxes along the trailing edge. Boxes other than on the trailing edge for wake contribution are given by

$$W_{Ki} = 0 \qquad 4.10$$

The final form for the solution of this problem is given by

$$\sum_i a_{Ki}\,\varphi_i = b_K \qquad 4.11$$

with

$$a_{Ki} = \delta_{Ki} - c_{Ki} - w_{Ki} \qquad 4.12$$

where δ_{ki} is the usual Kronecker Delta, viz.

$$\delta_{Ki} = 1 \qquad K = i$$

$$\delta_{Ki} = 0 \qquad K \neq i$$

4.3 Numerical Solution of the Potential Equation

The potential integral, as given by Eq. 4.1, contains a singularity in the ratio 1/r. As the point being evaluated, x, y, z, is approached by the dummy point of integration, x_1, y_1, z_1, r tends to zero and the integral becomes singular. This problem can be eliminated by the introduction of polar coordinates

$$dx\,dy = J\,dr\,d\theta$$

with the Jacobian given by

$$J = \left| \frac{d(X,Y)}{d(r,\theta)} \right| \qquad 4.13$$

Also to be considered are the singularities formed by the leading edge ($\frac{\partial \zeta}{\partial x} = \infty$) and the tip ($\frac{\partial S}{\partial y} = \infty$). These singularities are eliminated using the transformation given by Eq. 2.14. A method for eliminating both types of singularities simultaneously is shown in Appendix C.

Finally, Eq. 4.6 must be put into numerical form and the Gaussian parameters introduced. First consider the source coefficient, b_k

$$b_K = \iint \frac{1}{2\pi r} \frac{\partial \varphi}{\partial n} \, d\Sigma_i \qquad 4.14$$

with the upper surface given by the following:

$$S = z - z_u(x,y) = 0 \qquad 4.15$$

Rewriting Eq. 4.14 yields

$$b_K = -\iint \frac{1}{2\pi r} \frac{\partial S/\partial x}{|\nabla S|} dS \qquad 4.16$$

Introducing Eq. 4.15 gives

$$b_K = +\iint \frac{1}{2\pi r} \frac{\partial z_u}{\partial x} dx_1 dy_1 \qquad 4.17$$

Using Eqs. 2.13 and 2.14, Eq. 4.17 yields*

$$b_K = \iint \frac{1}{2\pi r} \frac{\partial z_u}{\partial x} \; c \, \frac{b}{2} \, 4 \bar{x}(1-\bar{y}) \, d\bar{x} \, d\bar{y} \qquad 4.18$$

For convenience, rewrite Eq. 4.18 as

$$b_K = \iint \bar{H}(\bar{x}, \bar{y}) \, d\bar{x} \, d\bar{y} \qquad 4.19$$

and finally, in suitable numerical form as

$$b_K = \sum \omega_{ij} \bar{H}(\bar{x}_i, \bar{y}_j) \qquad 4.20$$

*Note that the Jacobian of the combined transformation is given by $c \frac{b}{2} 4 \bar{x} \bar{y}$

where w_{ij}, X_j and Y_j are the Gaussian quadrature weights and abscissas.

In a similar manner, consider the doublet coefficients

$$C_{Kj} = \iint \frac{\partial}{\partial n} \left(\frac{1}{2\pi r} \right) d\Sigma \qquad 4.21$$

which can be rewritten as

$$C_{Kj} = -\iint \frac{\nabla S \cdot \nabla r}{|\nabla S| r^3} d\Sigma \qquad 4.22$$

Since using Eq. 4.15, $\frac{d\Sigma}{|\nabla S|} = dx_1\, dy_1$, the above equation can be rewritten as

$$C_{Kj} = -\iint \frac{\bar{\nabla} S \cdot \bar{\nabla} r}{r^3} dx_1 dy_1 \qquad 4.23$$

using Eqs. 2.13 and 2.14, one has

$$C_{Kj} = -\iint \left[\frac{\bar{\nabla} s \cdot \bar{\nabla} r}{r^3} c \frac{b}{a} \right. \qquad 4.24$$

$$\left. 4\bar{x}(1-\bar{y}) \right] d\bar{x}\, d\bar{y}$$

which, for convenience, can be written as

$$C_{Kj} = \iint \bar{\bar{H}}(\bar{x}, \bar{y})\, d\bar{x}\, d\bar{y} \qquad 4.25$$

Finally, Eq. 4.25 can be approximated in numerical form as

$$C_{Kj} \approx \sum_{ij} w_{ij} \bar{\bar{H}}(\bar{x}_i, \bar{y}_j) \qquad 4.26$$

Finally, the system given by Eq. 4.11 can be evaluated to form a system of N linear, simultaneous equations in N unknowns. For a high speed digital computer, the generation of this system is limited in the number N by the available computer storage. The solution can be obtained using Gaussian elimination with pivoting. Gaussian elimination is quite suitable to the solution of this system as there is the possibility of the matrix becoming singular. The subroutine used to apply the Gaussian method is not particular to the program devised but is the IBM subroutine "GELG".

Finally, the solution of the pressure distribution is obtained by taking the derivative of ϕ with respect to x as shown in Eq. 1.11.

5. NUMERICAL-ANALYTIC EVALUATION OF THE COEFFICIENTS

5.1 Introduction

The purely analytic method gives good results but only for thin wings. On the other hand, the purely numerical method gives good results but only for thick wings. A good method for evaluating moderately thick wings (i.e., wings of thicknesses in the range of those in practical use) should incorporate both methods. This combination is outlined in this Section.

5.2 Theory

This method is based on evaluating the surface both numerically and analytically to get the proper results. To begin, the body is approximated by tangent planes. To do this, first consider a tangent plane element in x, y, z so that z_0 is given by[3]

$$Z_0 = Z - \alpha x - \beta y \qquad 5.1$$

with the surface, S, given by

$$S = Z - \alpha x - \beta y - Z_0 = 0 \qquad 5.2$$

The exact expression for the doublet contribution is given by

$$C_{Kj} = -\iint \frac{\nabla S \cdot \nabla r}{r^3} \, dx_1 dy_1 \qquad 5.3$$

The expression for the doublet contribution in the tangent plane method is given by a similar expression as

$$(C_{Kj})_T = -\iint \left(\frac{\nabla S_T \cdot \nabla r_T}{r_T^3} \right) dx_1 dy_1 \qquad 5.4$$

with the subscript T indicating a "tangent plant" evaluation; in particular

$$\nabla S_T = \begin{Bmatrix} -\alpha \\ -\beta \\ 1 \end{Bmatrix} \qquad 5.5$$

The combination of these integrals, the difference integral, becomes

$$\Delta C_{Kj} = C_{Kj} - (C_{Kj})_T$$

$$= -\iint \left(\frac{\nabla S \cdot \nabla r}{r^3} - \frac{\nabla S_T \cdot \nabla r_T}{r_T^3} \right) dx_1 dy_1 \qquad 5.6$$

This integral is evaluated numerically using the method indicated in Section 4. In a similar manner, the correction to the source contribution is considered as

$$\Delta b_K = \iint \left[\frac{1}{2\pi r} \frac{\partial Z_u}{\partial x} - \frac{1}{2\pi r_T} \left(\frac{\partial Z_u}{\partial x} \right)_T \right] dx_1 dy_1 \qquad 5.7$$

also to be evaluated numerically. These differences will be added to the tangent plane approximation to yield a better estimate of the coefficients C_{kj} and b_k. It may be noted that higher numerical errors can now be tolerated since "errors on the correction" have small effect on the coefficients.

6. RESULTS AND CONCLUSIONS

6.1 Introduction

The three methods proposed, the modal method, the numerical method, and the analytical-numerical method, were programmed on a digital computer. Comparisons are made against experimental[4] and analytical results. The body surface used is a symmetrical wing at a 5° angle of attack (see Subsection 2.1).

6.2 Modal Method Results

The modal method yields good results but is limited in application with respect to the complexity of the body geometry involved. Numerical results obtained by using this method were very satisfactory for a good range of body thickness ratios. Comparison of the modal method is made with the analytical method using the same problem considered in Ref. 3. The problem is a rectangular wing in steady subsonic flow (Subsection 2.1). The number of modes used for the solution is four.

First, consider comparison with the box method[3]. Figures 9 and 10 show the comparison between the two methods in the chordwise and spanwise directions, respectively. Note that the slope of the diagrams for the box method and modal method compare favorably. Remember that the pressure distribution is the derivative of the potential so that the importance of the slope agreement can be brought into perspective.

Next, consider the convergence of the modal method in terms of the number of evaluation points. Figures 11 and 12 depict the convergence in terms of the number of points of evaluation on the body surface in the

chordwise and spanwise directions, respectively. Agreement here is extremely good. It may be noted that the solution using this method is a smooth curve and not discrete points. Points between the solution for six points show excellent agreement for five, four and even three points. Also, it is observed that fewer points describe the curve with less accuracy, but even for few points the agreement is still reasonably good.

Finally, the effect of the thickness ratio is considered. In Figs. 13 and 14 the convergence for body thickness ratios of .1, .01, and .001 is shown in the chordwise and spanwise directions, respectively. The results here are typical of those for the box method[3]. Again, the behavior here is what is expected as discussed in Subsection 6.2

Results for the modal method show it to be a reliable method for varying thickness ratios but, unfortunately limited in its use due to the difficulty in "guessing" the shapes of the potential, and thus the modes, for complex geometries (i.e., wing-body interference). Furthermore, the computer time is much longer than for the box method. Hence, as mentioned above, the box method is considered to be superior and was investigated more deeply.

6.3 Analytic-Numerical Results

The analytical-numerical method provides very satisfactory results in a varying range of thickness ratios. It is the varying range of

applicability with respect to body thicknesses that makes this method so desirable.

The analytical-numerical method is compared here with experiments and also with the purely analytical method in order to evaluate the improvement. Furthermore, the convergence of the method and the thickness effects are also examined.

Figure 15 shows a comparison of the analytical method, the analytical-numerical method and experiments using the wing in Subsection 2.1 at an angle of attack of 5° and a thickness ratio of 1%. Results here show that the analytical-numerical method provides a good description of the pressure distribution with respect to experiments and therefore, the lift, the area under the pressure diagram, is also described well. Note also that both the analytical and the analytical-numerical methods compare favorably.

Next consider the convergence with respect to the number of points of solution on the body surface. Since the solution is a solution of discrete points it is necessary to check that when the number of points of evaluation is changed, the solution converges to the same curve. This is shown in Figs. 16 and 17 for various numbers of points in the spanwise and chordwise directions, respectively. For a wing with six points of evaluation connected by a smooth curve it is evident from Figs. 16 and 17 that the solution based on 3, 4 and 5 points lies satisfactorily on the same curve.

Finally, consider the influence of body thickness on the results. Here the potential is plotted in the spanwise and chordwise directions in Figs. 18 and 19, respectively. The thickness ratio is varied in these figures from .001 to .1. The behavior is as expected. Note that at the tip and leading edge, the variation is small, while at the root and trailing edge the variation is larger.

In summary, it is evident that the analytical-numerical method provides good results for a large range of thickness ratios. Note that a body thickness ratio of .1 is a wing with maximum body thickness to wing chord ratio of 10%, well within practical body thickness ratios. Since the method is also convergent, it has proven to be quite a reliable and accurate method.

6.4 Suggestions for Further Study

The geometry evaluated in this thesis are of the most simple case, a symmetrical wing at a small angle of attack. Obviously, this geometry was chosen for its simplicity in testing the methods as it is easier to program and debug. It is also quite obvious that the most advantageous quality of this method is the evaluation of complicated geometries to include the problem of wing-body interference. It is therefore suggested that a study of complicated geometries be made using the analytical-numerical method.

Because of the nature of the formulation of the problem, it is by no means restricted to steady, incompressible flow as considered by this thesis. It is suggested that the numerical formulation be extended to include unsteady compressible (subsonic and supersonic) flow-fields.

REFERENCES

1. Ashley, H., and Landahl, M. T., Aerodynamics of Wings and Bodies, Addison-Wesley Publ. Co., 1965.
2. Ashley, H., and Rodden, W. P., "Wing Body Aerodynamic Interaction," Annual Review of Fluid Mechanics, Vol. 4, 1972, pp. 431-472.
3. Morino, L., "Unsteady Compressible Potential Flow Around Lifting Bodies Having Arbitrary Shapes and Motions," TR-72-01, Department of Aerospace Engineering, Boston University, 1972.
4. Cunningham, A. M. Jr., "An Efficient, Steady Subsonic Collocation Method for Solving Lifting-Surface Problems," J. Aircraft, Vol. 8, No. 3, March 1971, pp. 168-176.
5. Lessing, H. C., Troutman, J. C. and Menees, G. P., "Experimental Determination of the Pressure Distribution on a Rectangular Wing Oscillating in the First Bending Mode for Mach Numbers from 0.24 to 1.30," NASA TN D-344, 1960.
6. Abramowitz, M., and Stegun, I. A., "Handbook of Mathematical Functions," Dover Publ. Co., 1965, pp. 916-919.

FIGURES

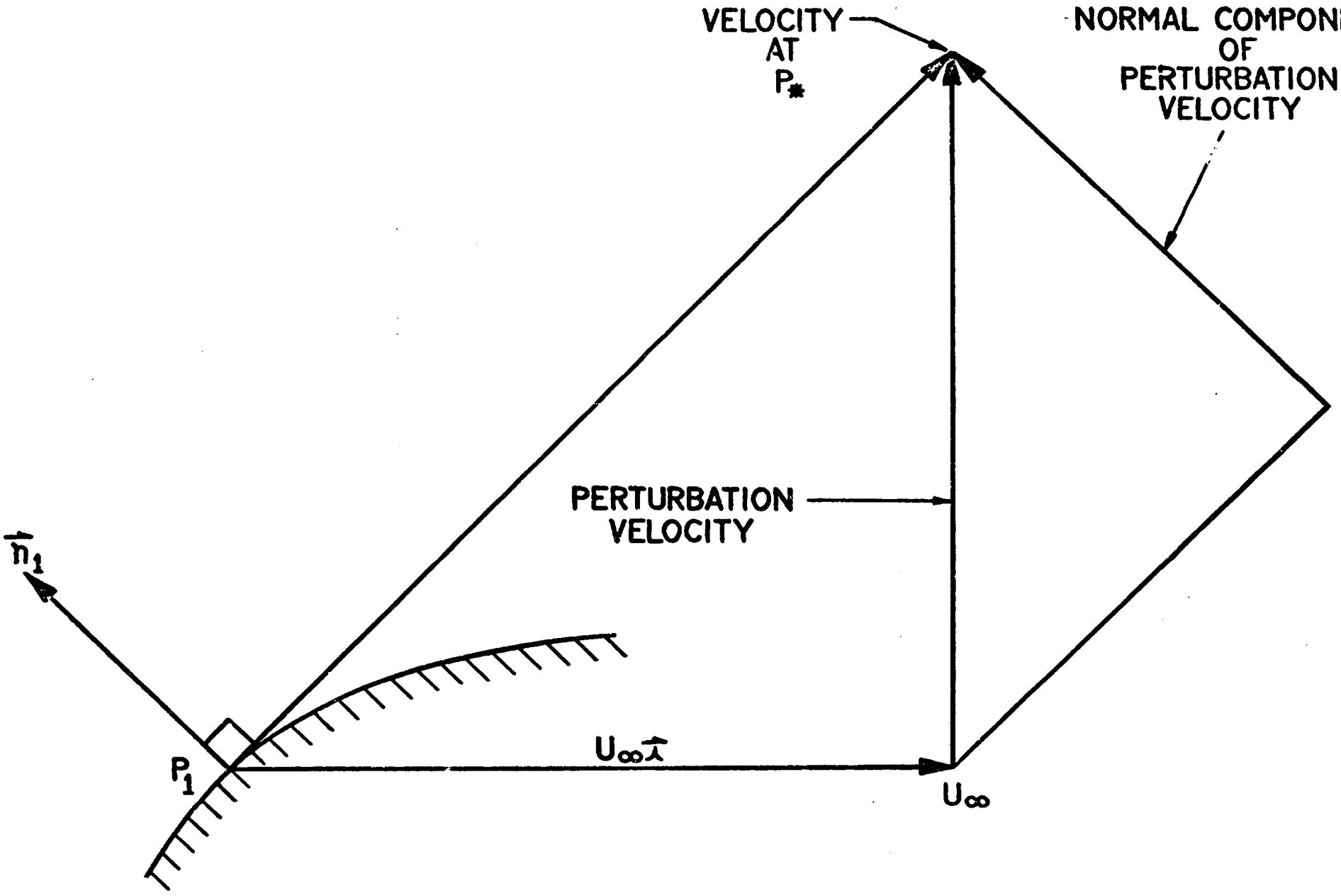

BOUNDARY CONDITIONS
FIGURE 1

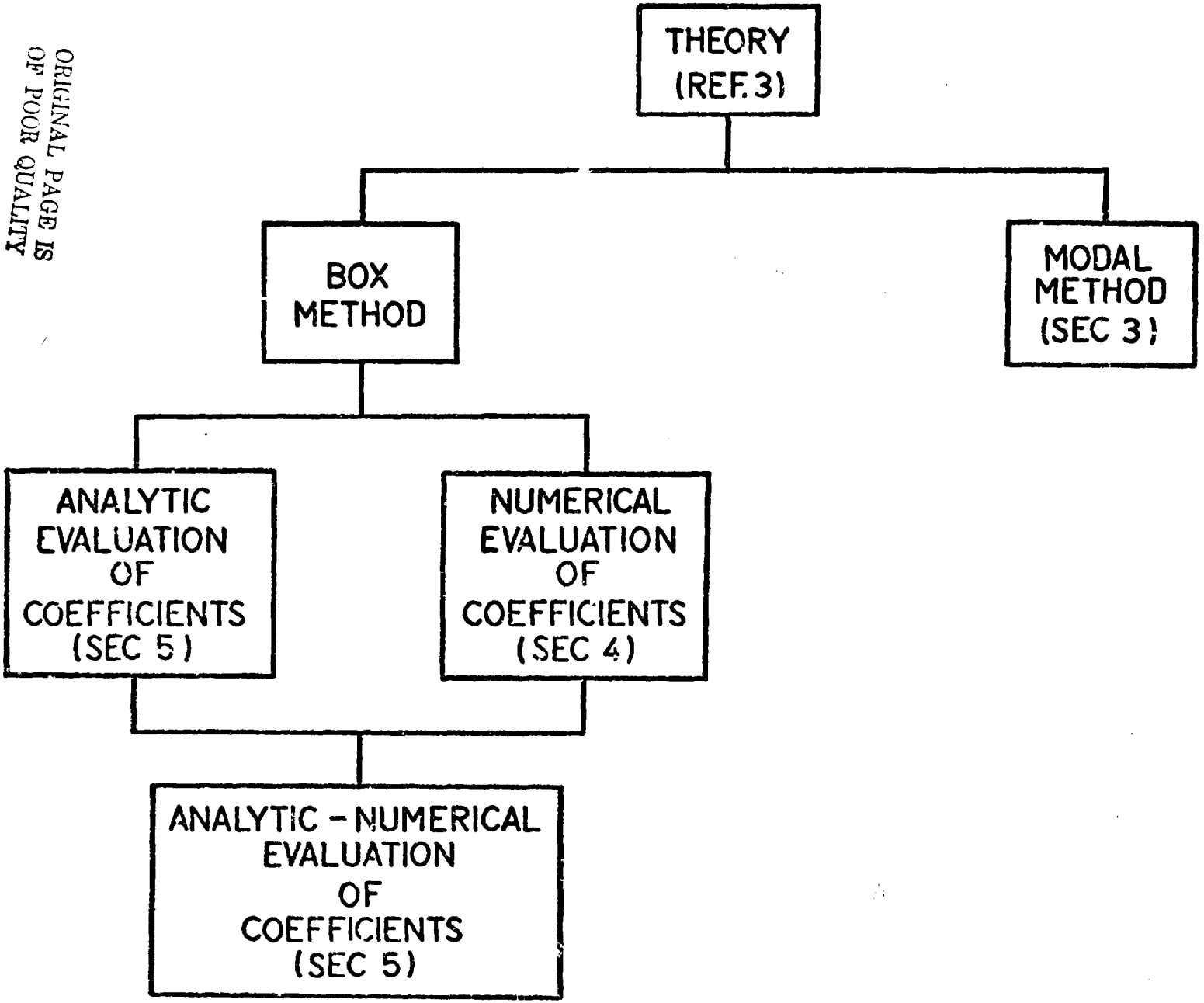

METHOD DEVELOPMENT FLOW CHART
FIGURE 2

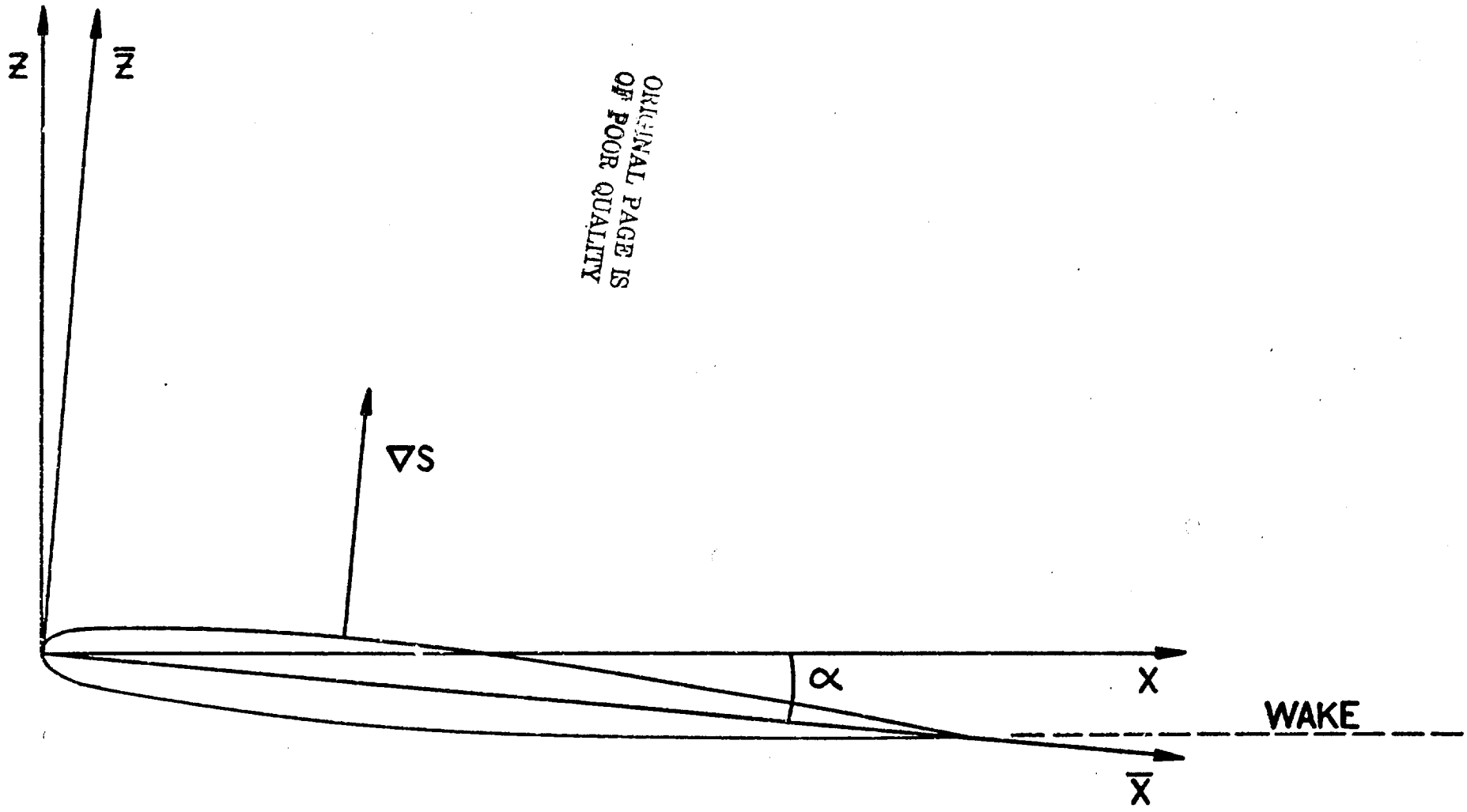

GEOMETRY OF THE PROBLEM
FIGURE 3

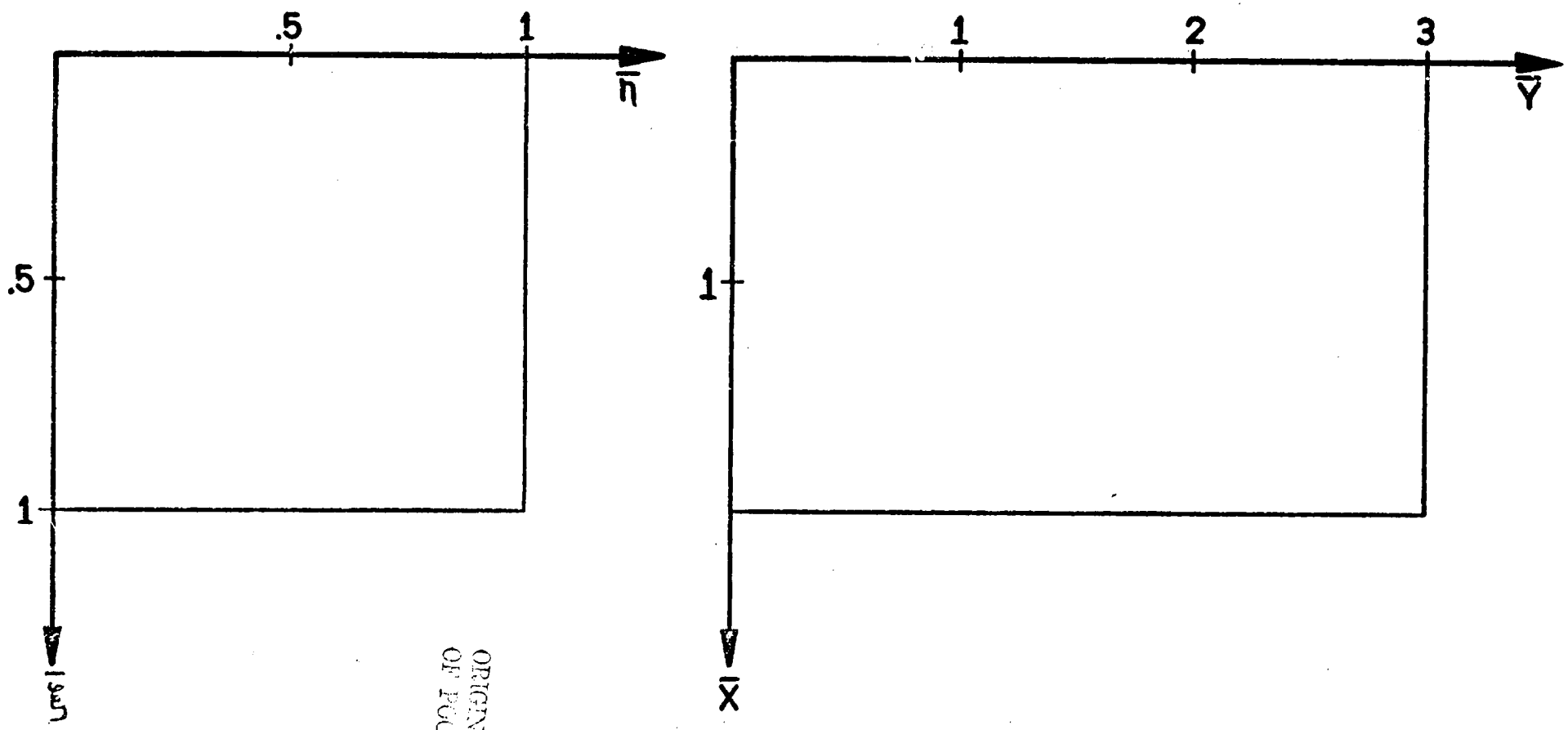

RECTANGULAR WING AND COORDINATES
FIGURE 4

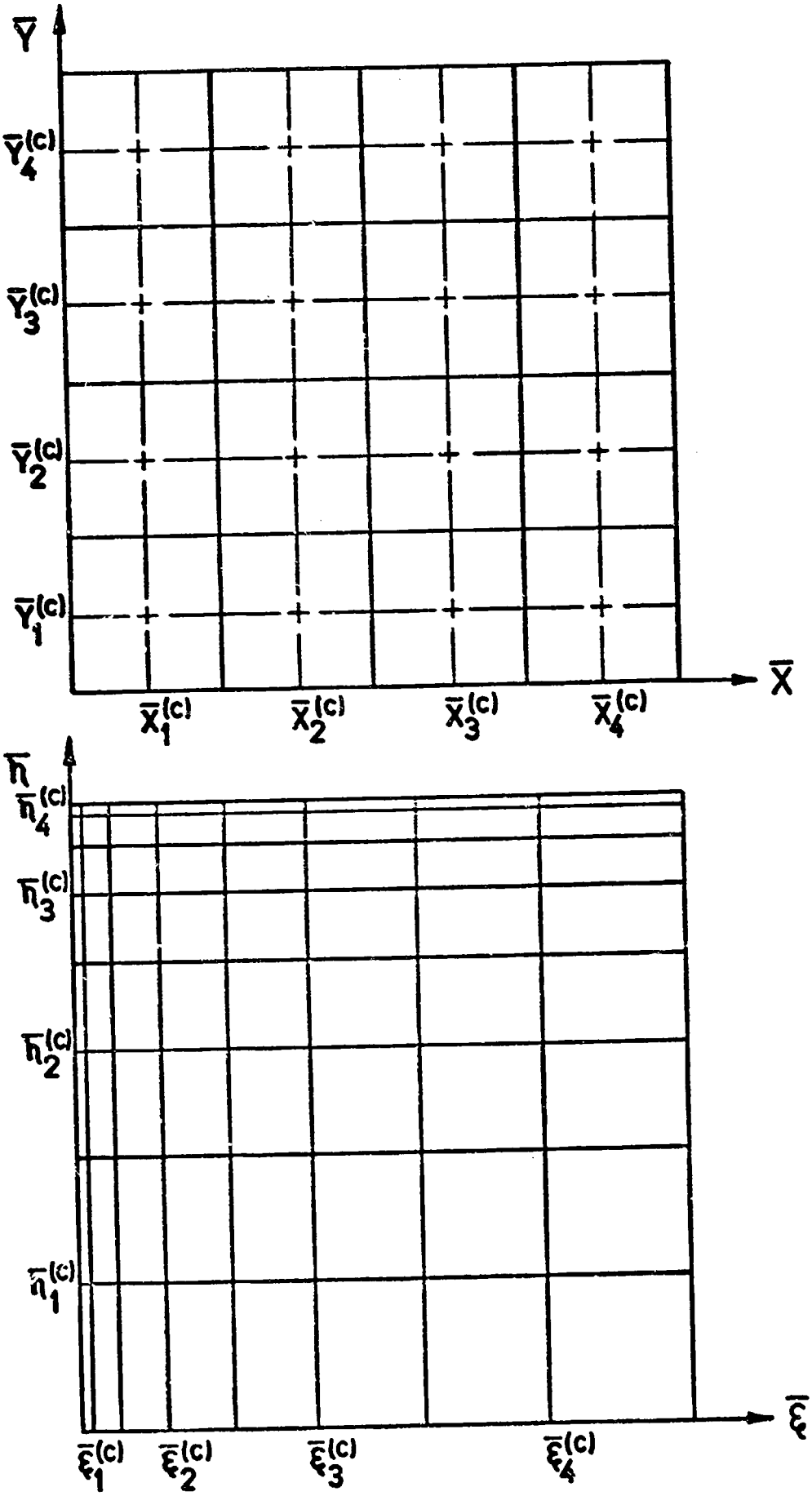

LEADING EDGE AND TIP EMPHASIS DIAGRAM
FIGURE 5

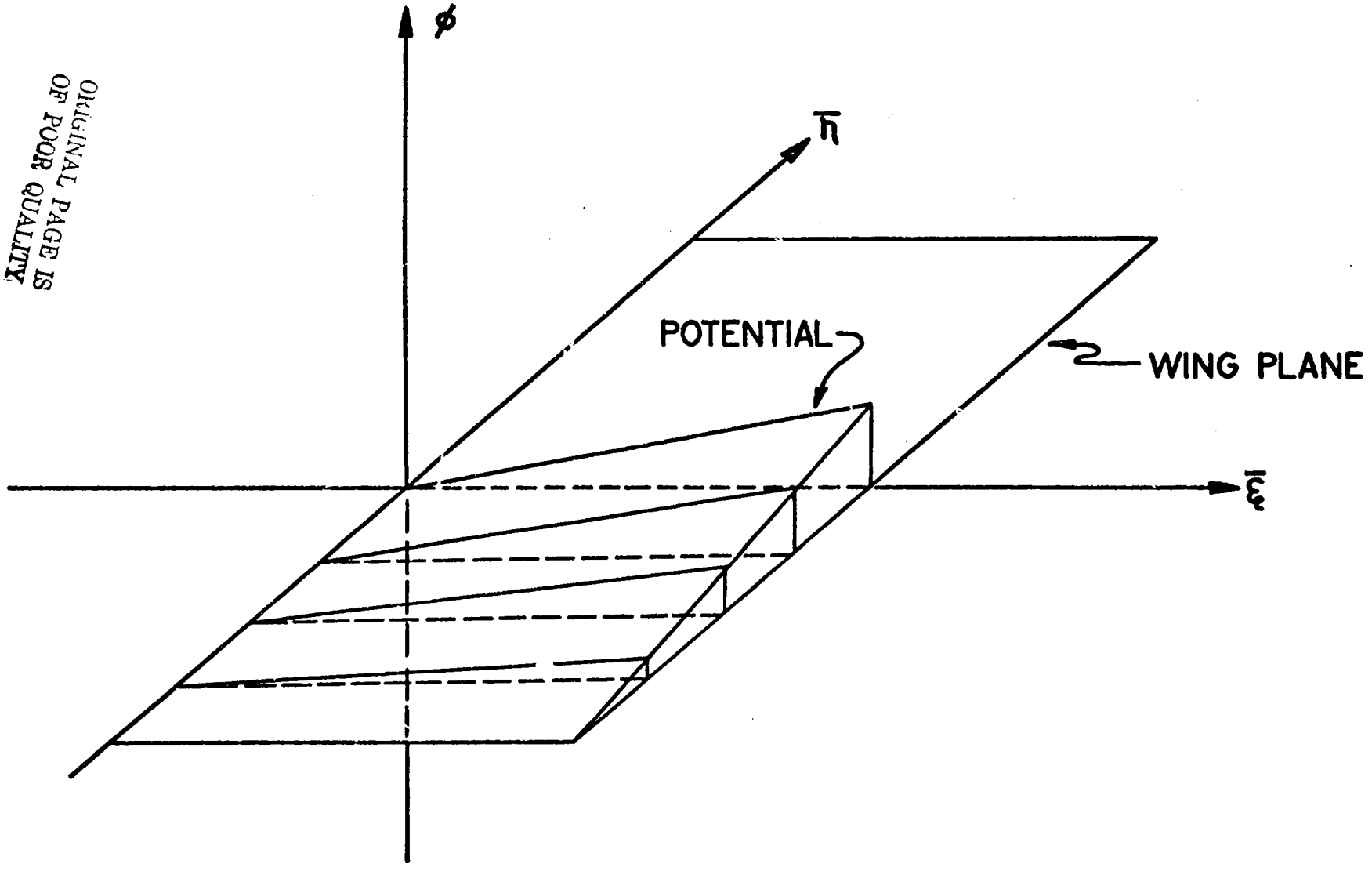

SYMMETRICAL COMPONENT OF POTENTIAL
FIGURE 6a

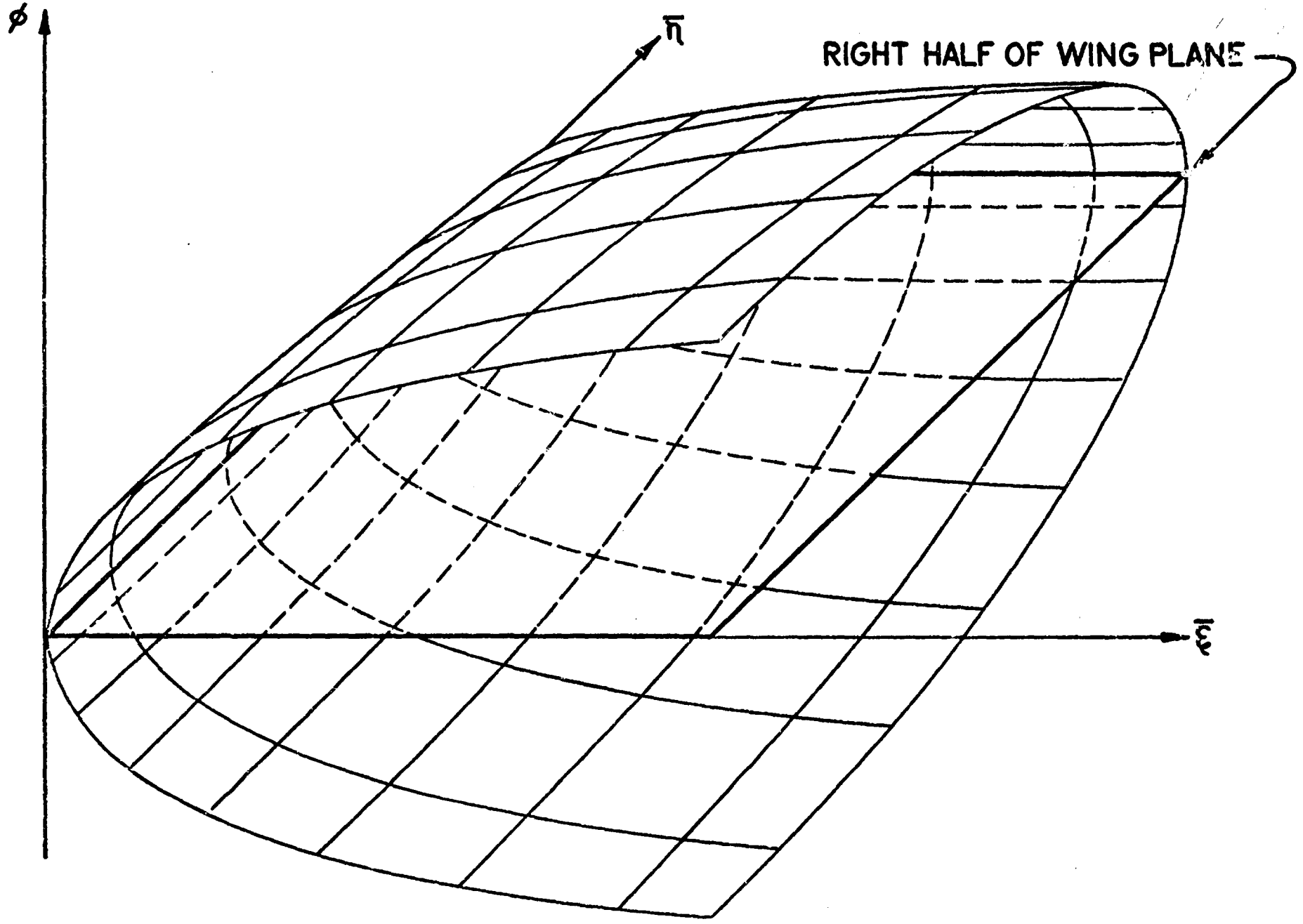

ANTI-SYMMETRICAL COMPONENT OF THE POTENTIAL

FIGURE 6b

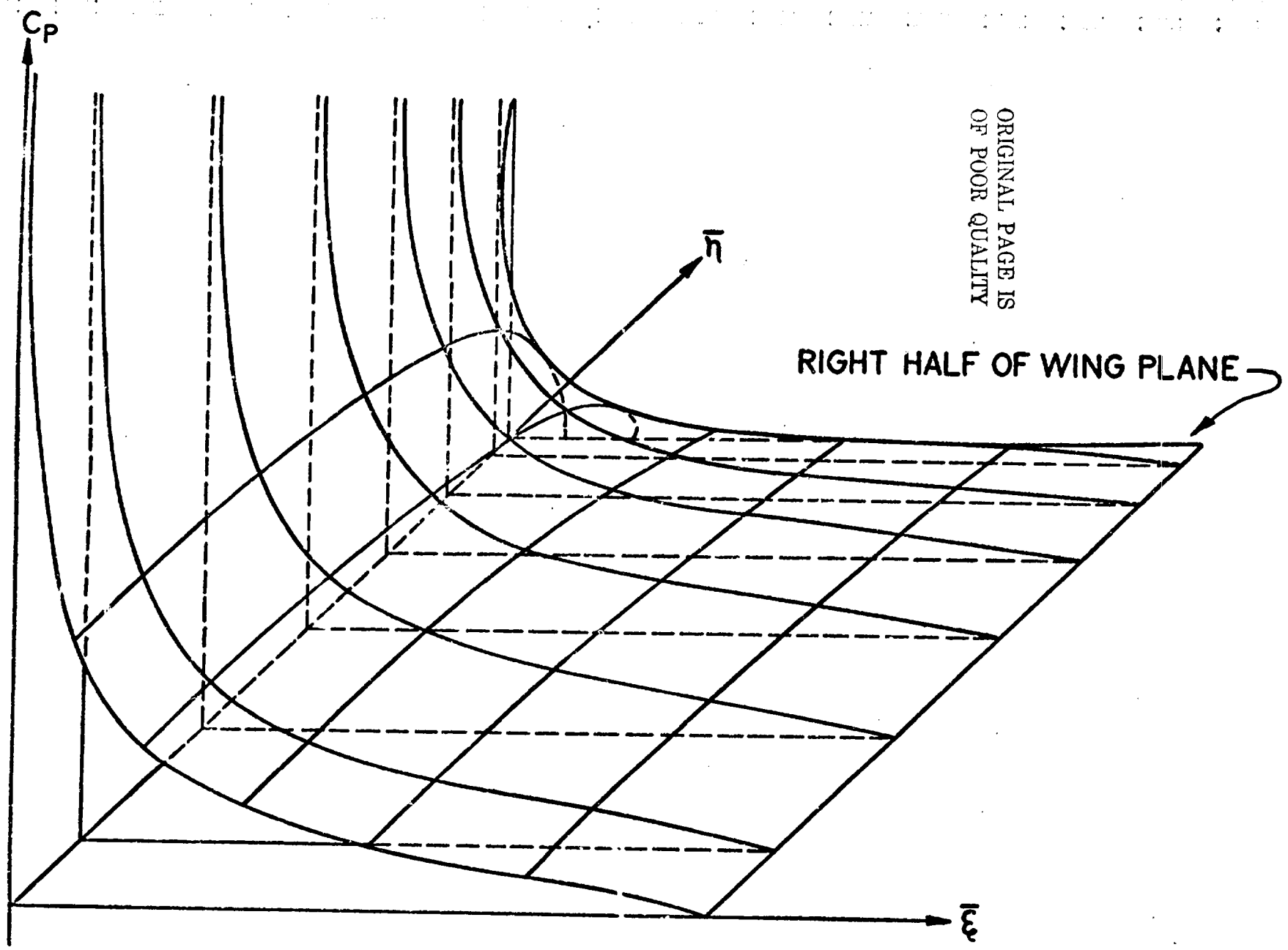

SHAPE OF PRESSURE DISTRIBUTION
FIGURE 7

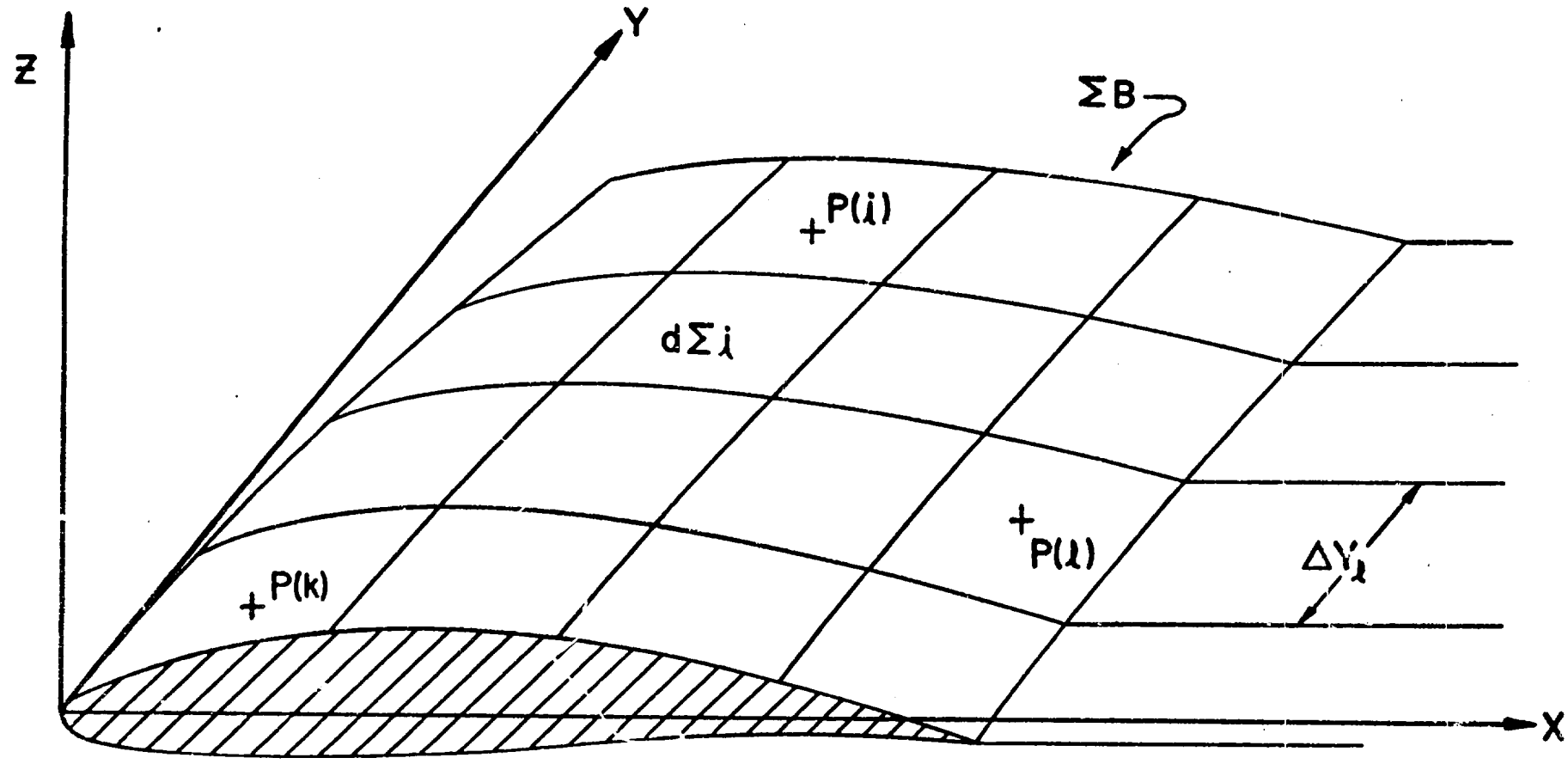

BODY SUB-ELEMENTS
FIGURE 8

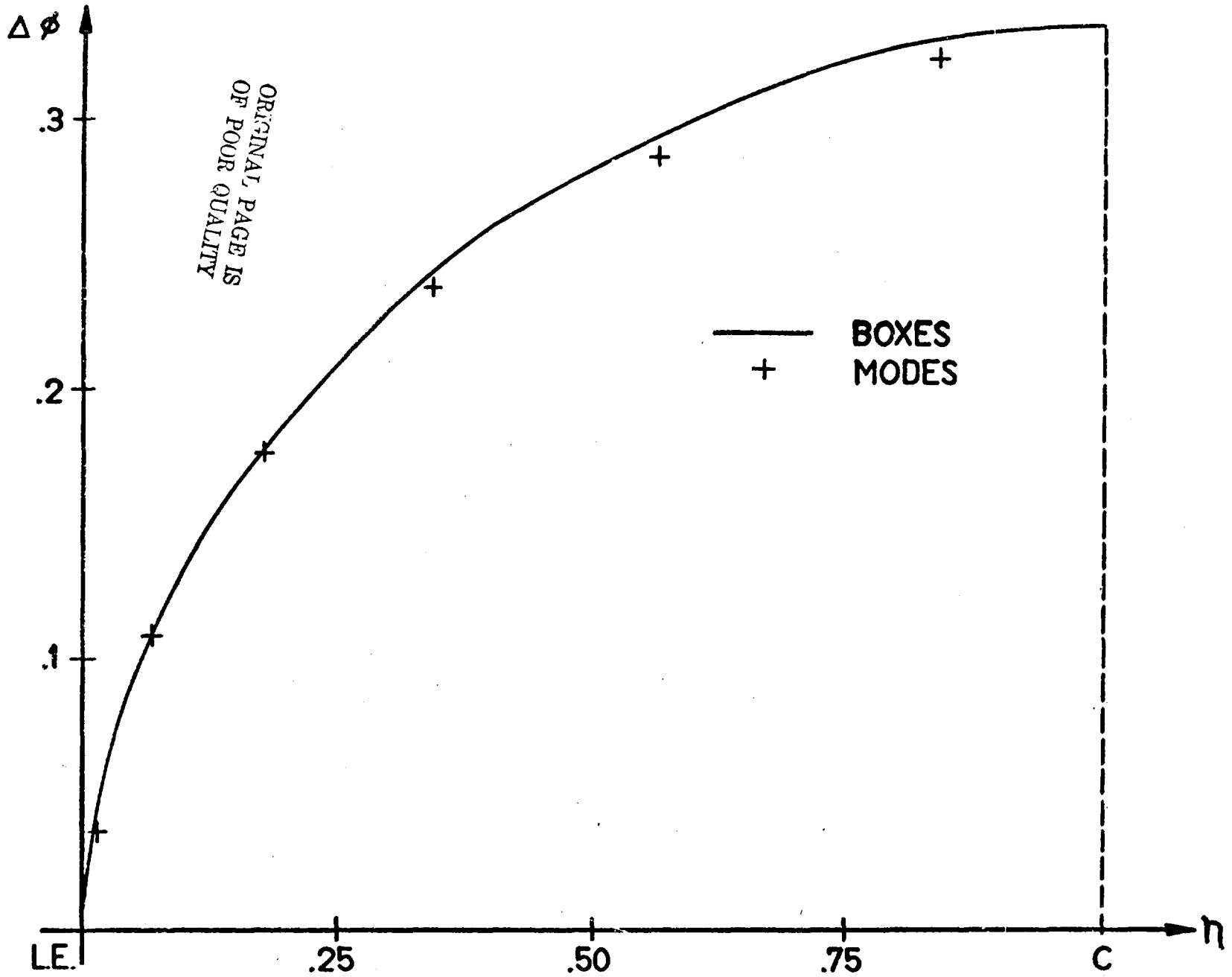

COMPARISON OF BOX AND MODE METHODS, CHORDWISE
FIGURE 9

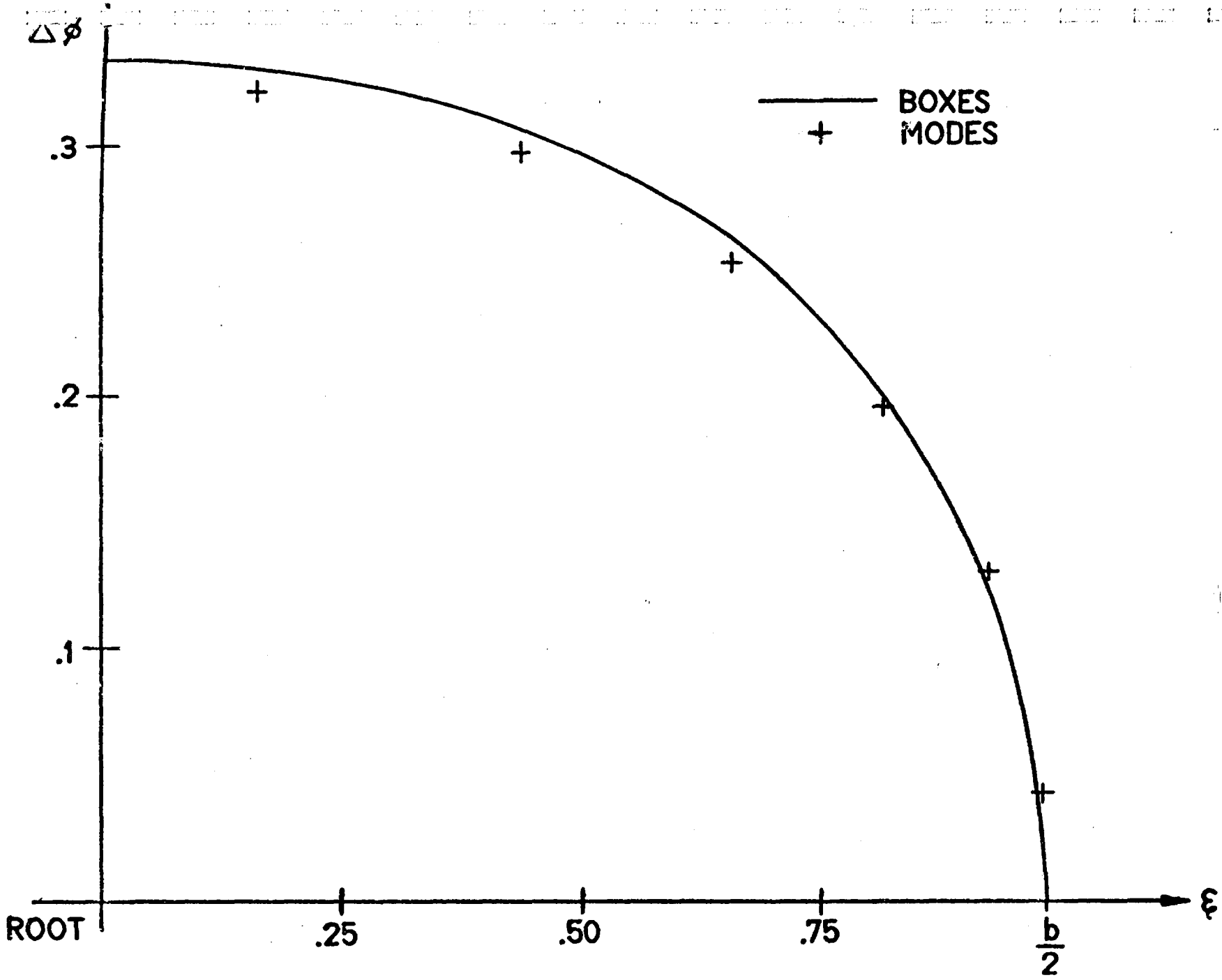

COMPARISON OF BOX AND MODAL METHODS, SPANWISE

FIGURE 10

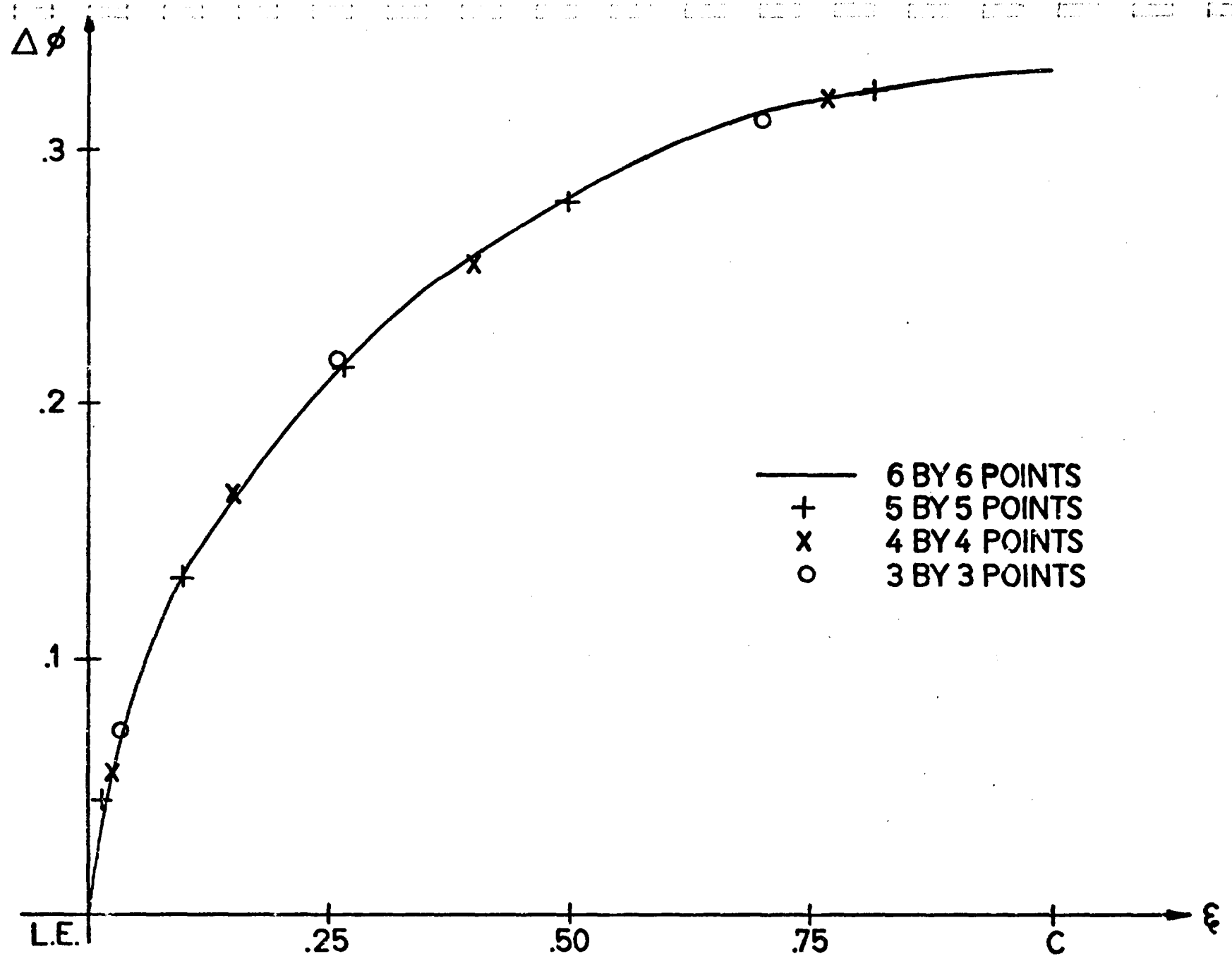

POTENTIAL (MODAL) CONVERGENCE WRT NUMBER OF SURFACE POINTS, CHORDWISE

FIGURE 11

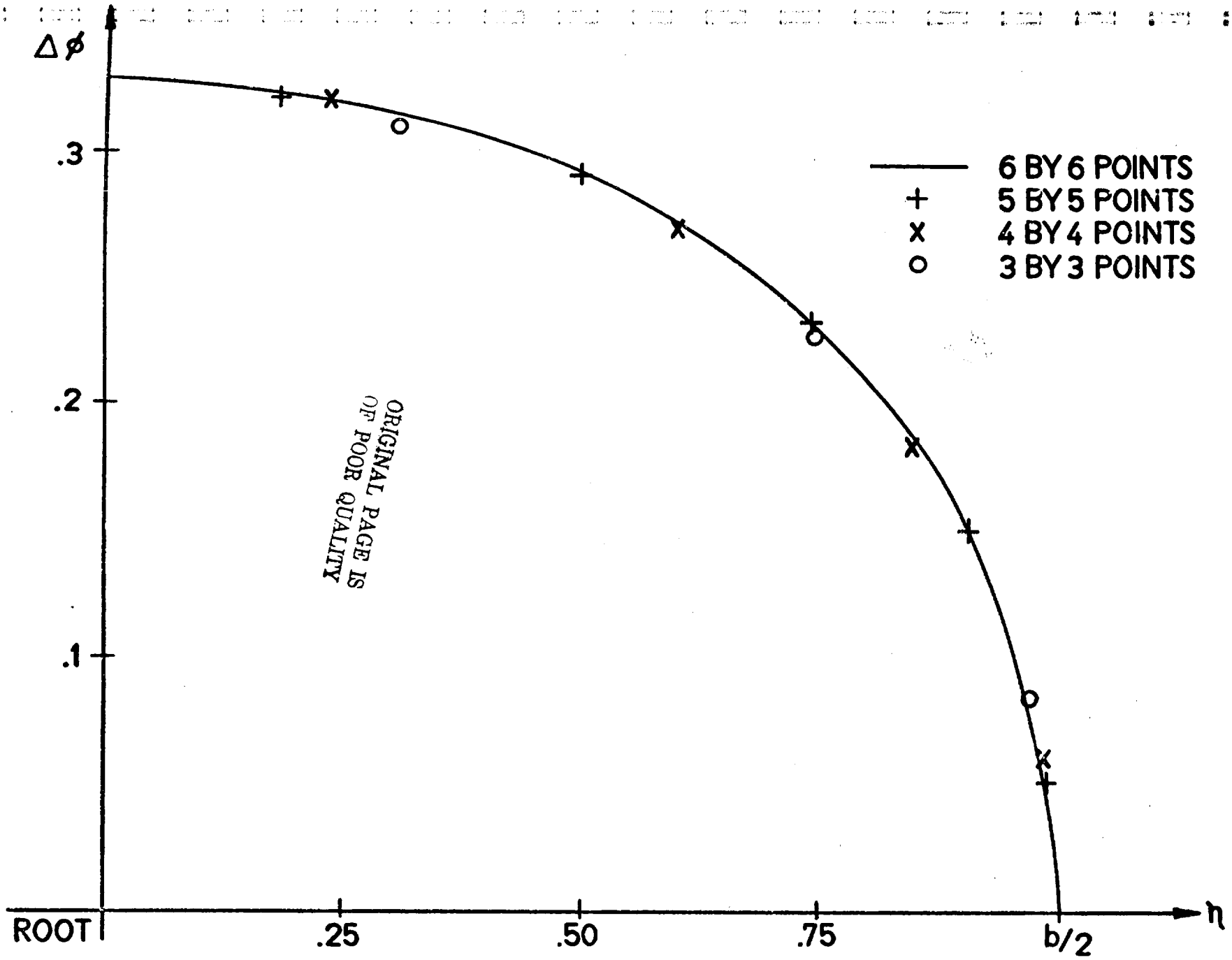

POTENTIAL (MODAL) CONVERGENCE WRT NUMBER OF SURFACE POINTS, SPANWISE

FIGURE 12

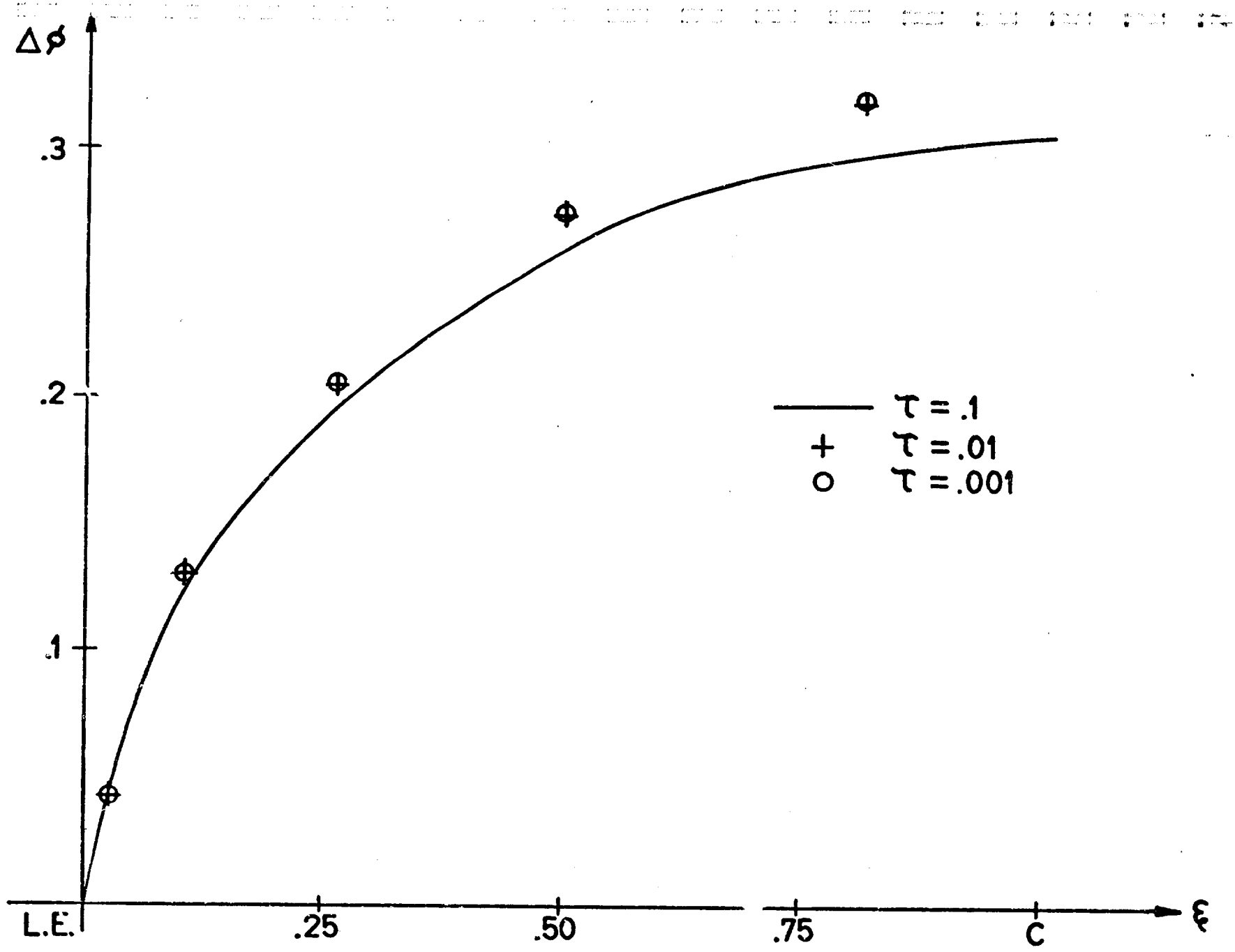

POTENTIAL (MODAL) CONVERGENCE WRT BODY THICKNESS RATIO

FIGURE 13

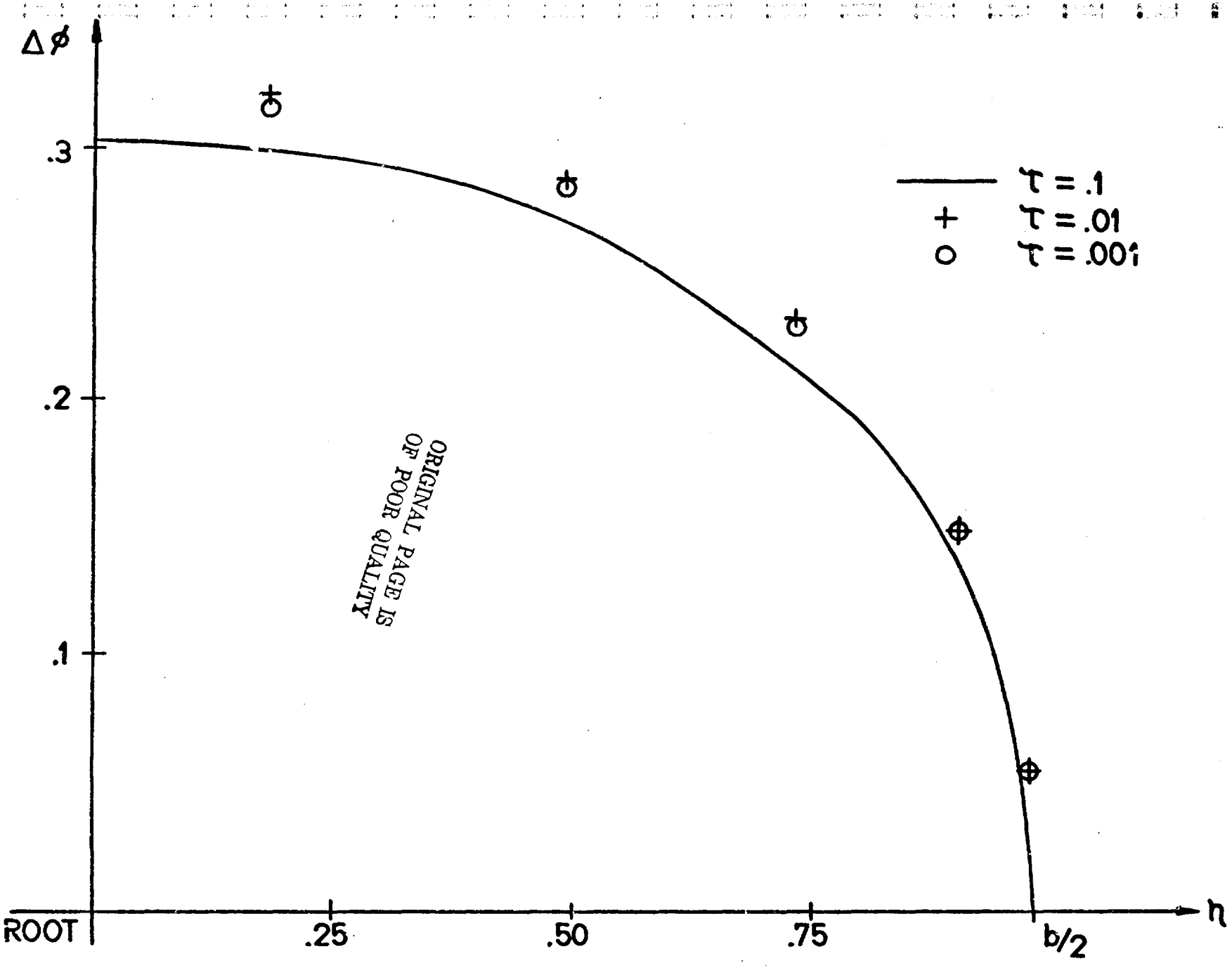

POTENTIAL (MODAL) CONVERGENCE WRT BODY THICKNESS RATIO
FIGURE 14

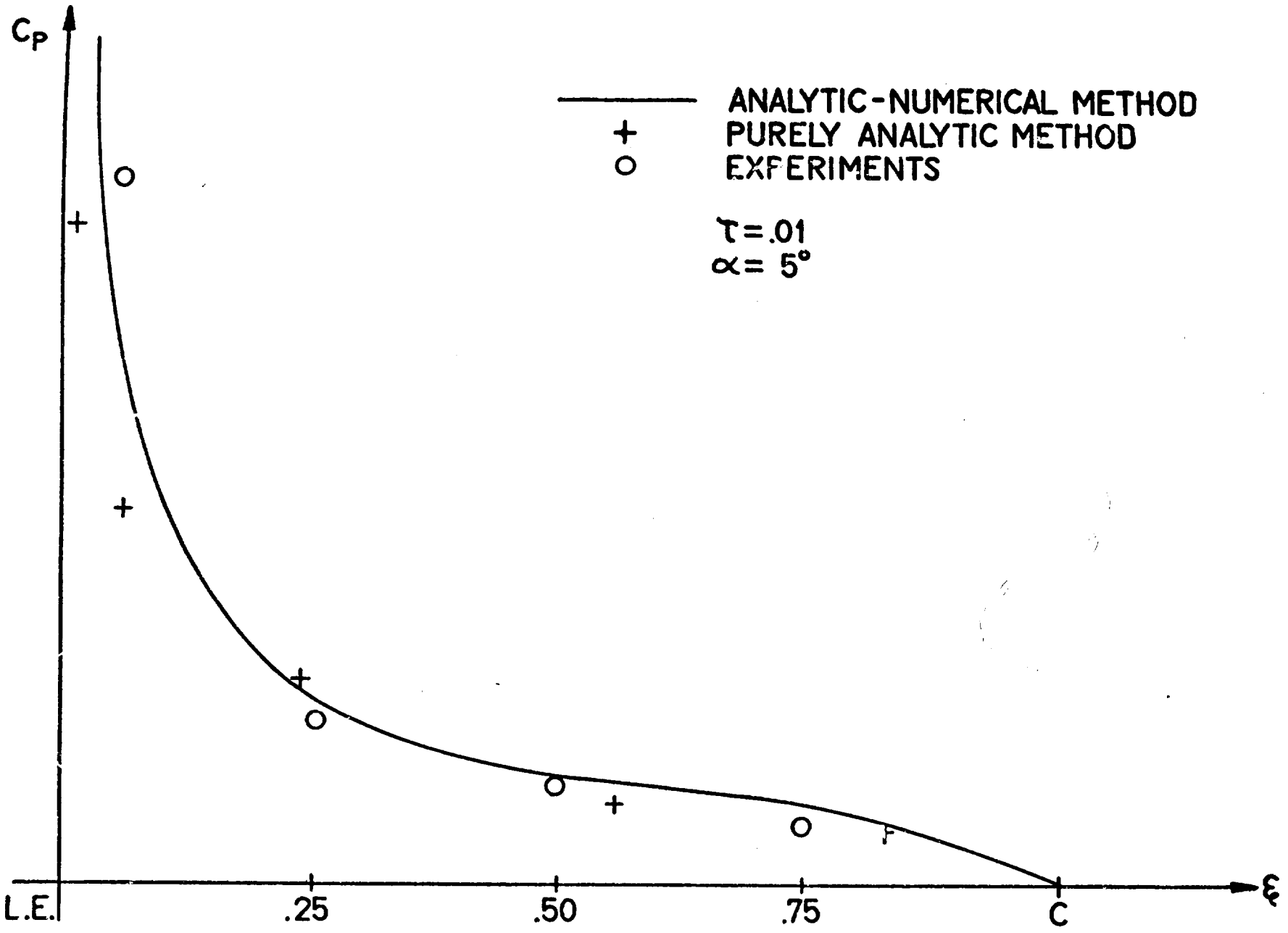

PRESSURE DISTRIBUTION, CHORDWISE DIRECTION

FIGURE 15

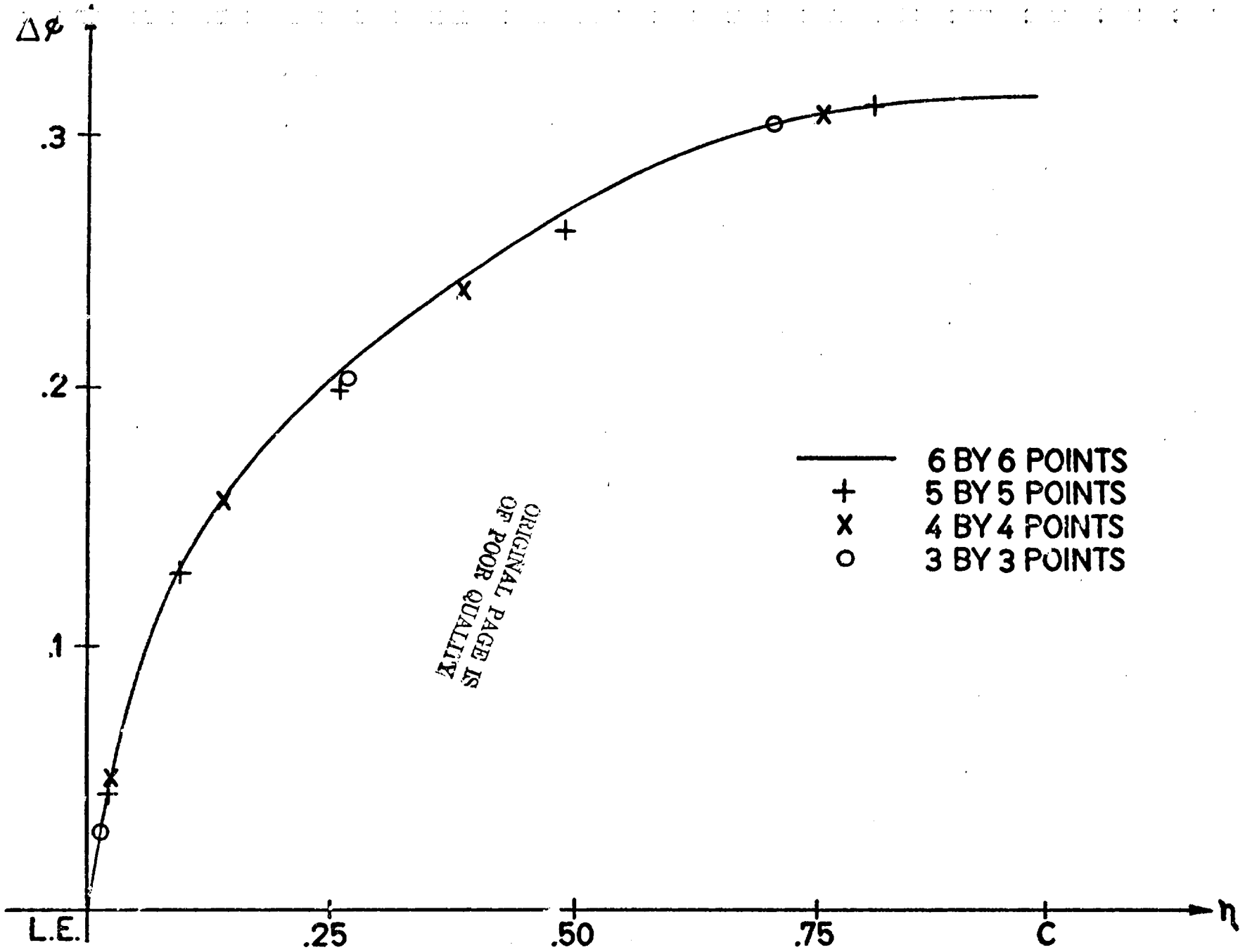

POTENTIAL (ANAL-NUM) CONVERGENCE WRT NUMBER OF SURFACE POINTS, CHORDWISE

FIGURE 16

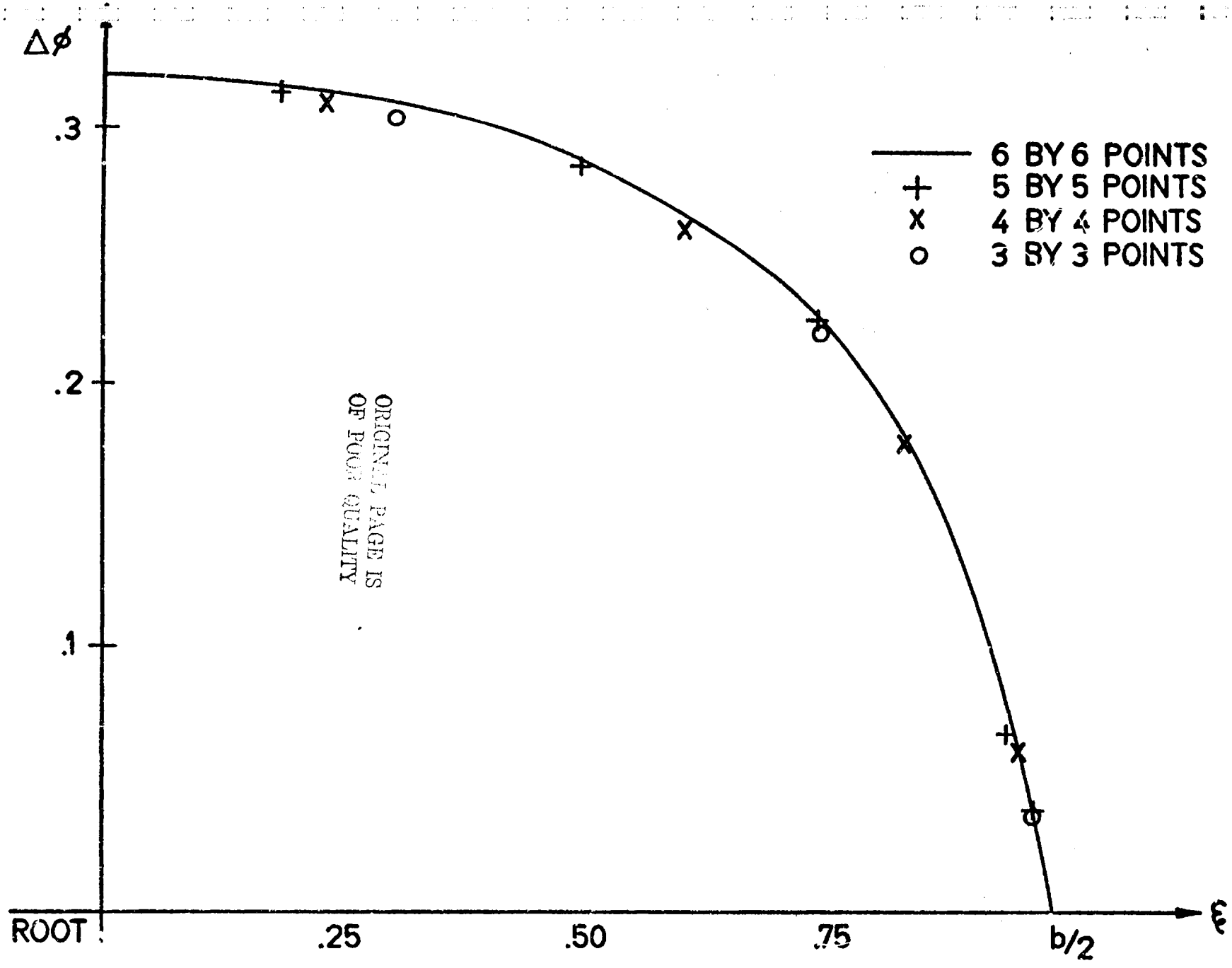

POTENTIAL (ANAL-NUM) CONVERGENCE WRT NUMBER OF SURFACE POINTS, SPANWISE

FIGURE 17

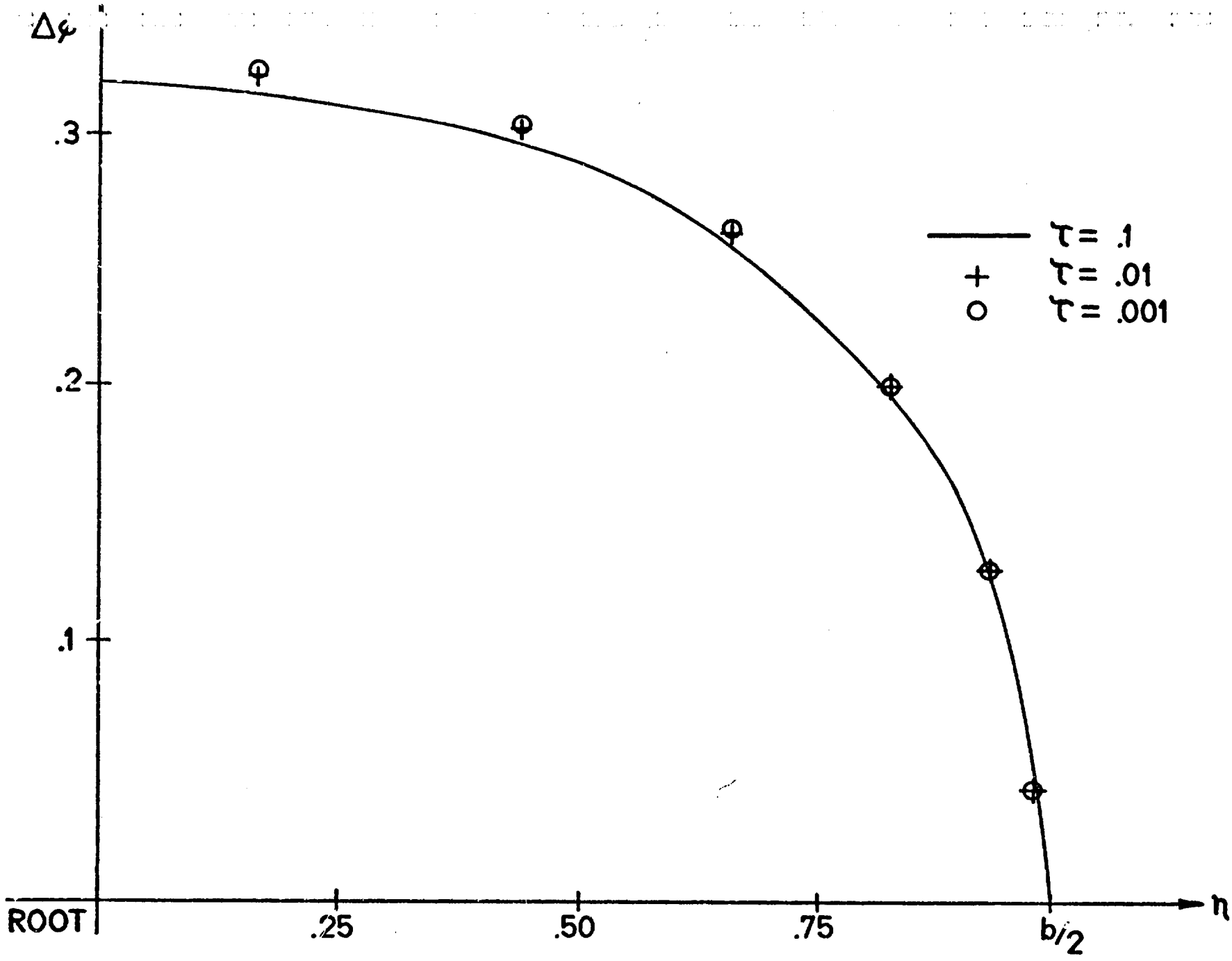

POTENTIAL (ANAL-NUM) CONVERGENCE WRT BODY THICKNESS, SPANWISE

FIGURE 18

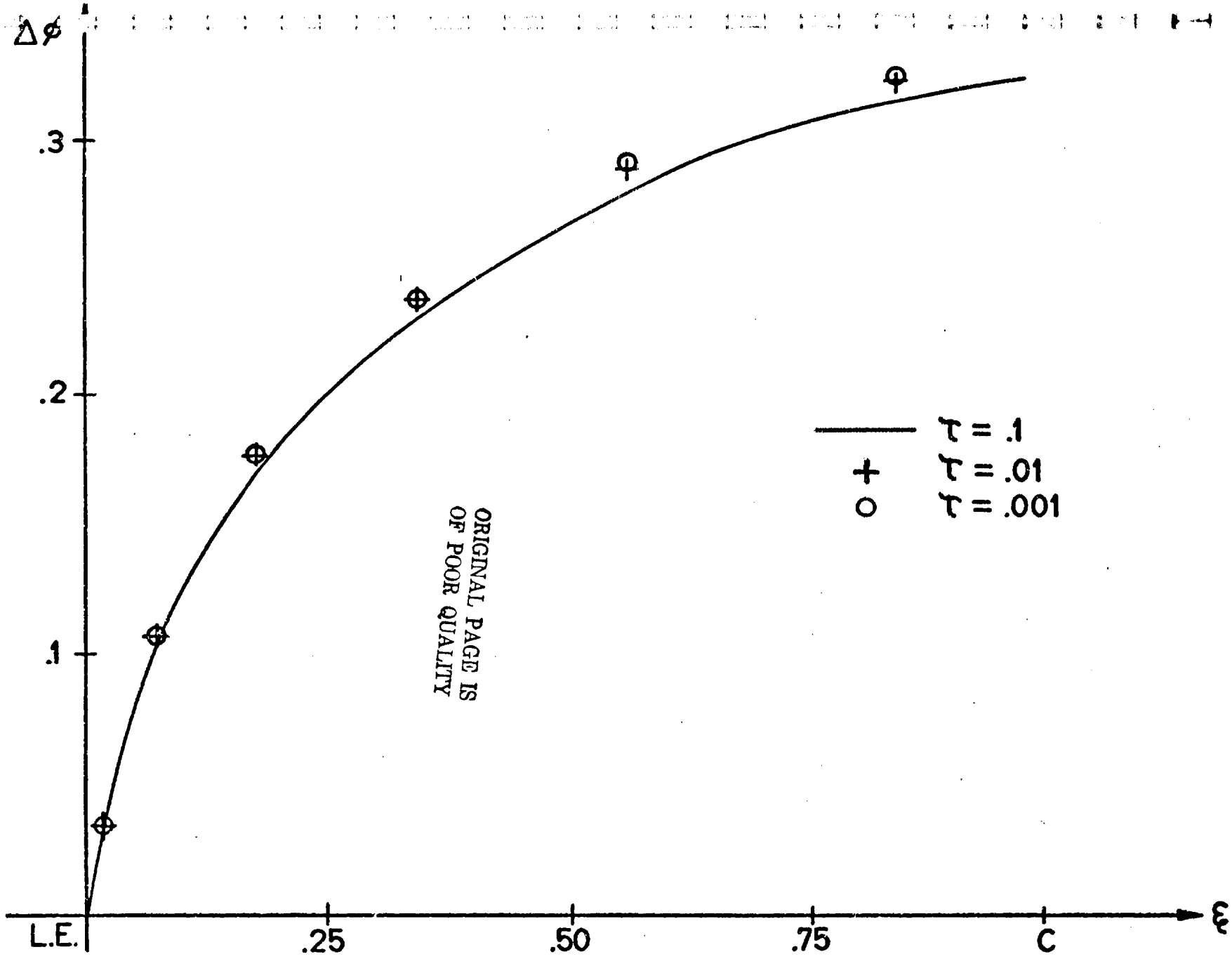

POTENTIAL (ANAL-NUM) CONVERGENCE WRT BODY THICKNESS, CHORDWISE

FIGURE 19

APPENDIX A

DERIVATION OF THE INTEGRAL POTENTIAL EQUATION ON THE BODY SURFACE

For the sake of completeness in this appendix, the derivation of Eq. 1.12 (Ref. 3) is summarized. For convenience, Eq. 1.12 is given here as:

$$\varphi(X,Y,Z) = -\iint_{\Sigma} \frac{\partial \varphi}{\partial n_1}(X_1,Y_1,Z_1)\frac{1}{4\pi r}\,d\Sigma + \iint_{\Sigma} \varphi(X_1,Y_1,Z_1)\frac{1}{4\pi r}\,d\Sigma \qquad \text{A.1}$$

where

$$r = \left[(X-X_1)^2 + (Y-Y_1)^2 + (Z-Z_1)^2\right]^{1/2} \qquad \text{A.2}$$

When the point P is allowed to approach the point P_*, as shown in Fig. A1, the integrands of Eq. A.1 become singular. In order to perform the limit it is convenient to isolate a neighborhood about P_* having area σ and radius ε. With this in mind, rewrite Eq. A.1 as:

$$\varphi(x_1,y_1,z_1) = -\iint_{\Sigma-\sigma} \frac{\partial \varphi}{\partial n}(x_1,y_1,z_1)\,\frac{1}{4\pi r}\,d\Sigma$$

$$-\iint_{\sigma} \frac{\partial \varphi}{\partial n}(x_1,y_1,z_1)\frac{1}{4\pi r}\,d\Sigma + \iint_{\Sigma-\sigma} \varphi(x_1,y_1,z_1)\frac{\partial}{\partial n}\left(\frac{1}{4\pi r}\right)d\Sigma$$

$$+\iint_{\sigma} \varphi(x_1,y_1,z_1)\,\frac{\partial}{\partial n}\left(\frac{1}{4\pi r}\right)d\Sigma$$

$$= I_S' + I_S'' + I_D' + I_D''$$

With obvious definitions of I_S', I_S'' and I_D''.

First consider the doublet integral

$$I_D = I_D' + I_D'' \qquad \text{A.3}$$

Consider a local coordinate system ξ, η, ζ as shown in Fig. A2 in order to evaluate I_D''. Assume the area σ to be circular having radius ϵ, so small that σ can be replaced by its tangent plane. Rewriting I_D'' in the new variables yields:

$$I_D'' = -\int_0^{2\pi}\int_0^{\varepsilon} \varphi \left[\frac{\partial}{\partial \zeta}\left(\frac{1}{4\pi r}\right)\right]_{\zeta_1=0} \rho\, d\rho\, d\alpha \qquad \text{A.4}$$

where $\rho^2 = \xi_1^2 + \eta_1^2$ and α is shown in Fig. A3. Note that

$$\begin{aligned} r^2 &= (x_1 - x)^2 + (y_1 - y)^2 + (z_1 - z)^2 \\ &= \xi_1^2 + \eta_1^2 + (\zeta_1 - \zeta_*)^2\Big|_{\zeta_1=0} \qquad \text{A.5} \\ &= \rho^2 + \left[(\zeta_1 - \zeta)^2\right]\Big|_{\zeta_1=0} \end{aligned}$$

Next consider

$$\frac{\partial}{\partial \zeta_1}\left(\frac{1}{4\pi r}\right)\Big|_{\zeta_1=0} = -\frac{1}{2}\frac{z_1(\zeta_1 - \zeta)}{4\pi r^3}\Big|_{\zeta_1=0}$$

$$= \frac{\zeta}{4\pi r^3}$$

and

$$\frac{\partial}{\partial \rho}\left(\frac{1}{4\pi r}\right) = -\frac{1}{2}\,\frac{2\rho}{4\pi r^3}$$

$$= -\frac{\rho}{4\pi r^3}$$

Combining yields

$$\left.\frac{\partial}{\partial \xi_1}\left(\frac{1}{4\pi r}\right)\right|_{\xi_1=0} = -\frac{\xi}{\rho}\,\frac{\partial}{\partial \rho}\left(\frac{1}{4\pi r}\right) \qquad \text{A.6}$$

Using A.6, Eq. A.4 becomes

$$I''_D = -\xi \int_0^{2\pi} \int_0^{\varepsilon} \rho\,\frac{\partial}{\partial \rho}\left(\frac{1}{4\pi r}\right) d\rho\, d\alpha \qquad \text{A.7}$$

For very small ε, φ is nearly constant and can be replaced under this assumption by its value at the point x_*, y_*, z_* as

$$\varphi_* = \varphi(X_*, Y_*, Z_*)$$

Equation A.7 now becomes

$$I_D'' = -\zeta \varphi_* 2\pi \int_0^{\varepsilon} \frac{\partial}{\partial \rho}\left(\frac{1}{4\pi r}\right) d\rho$$

$$= -2\pi \zeta \varphi_* \left[\frac{1}{4\pi r}\right]\Bigg|_{\rho=0}^{\rho=\varepsilon} \qquad \text{A.8}$$

$$= \frac{\varphi_*}{2}\left(1 - \frac{\zeta}{\sqrt{\varepsilon^2 + \zeta^2}}\right)$$

As ζ goes to zero, i.e., x, y, z approaches x_*, y_*, z_*, Eq. A.8 becomes

$$\lim_{(X,Y,Z)\to(X_*,Y_*,Z_*)} I_D'' = \lim_{\zeta \to 0}\left[\frac{\varphi_*}{2}\left(1 - \frac{\zeta}{\sqrt{\varepsilon^2 + \zeta^2}}\right)\right]$$

$$\lim_{(X,Y,Z)\to(X_*,Y_*,Z_*)} I_D'' = \frac{\varphi_*}{2} \qquad \text{A.9}$$

Combining Eqs. A.3 and A.9 and applying the limit as $P \to P_*$ yields

$$\lim_{P\to P_*} I_D = \frac{\varphi_*}{2} + \lim_{\varepsilon\to 0} \iint_{\Sigma-\sigma_\varepsilon} \varphi \frac{\partial}{\partial n_1}\left(\frac{1}{4\pi r_*}\right) d\Sigma \qquad \text{A.10}$$

with

$$r_* = \left[(X_* - X_1)^2 + (Y_* - Y_1)^2 + (Z_* - Z_1)^2 \right]^{1/2}$$

Similar treatment of the sources yields no special contribution from the neighborhood of P_*.[3] Equation A.1 can now be written as:

$$\varphi(P_*) = -\iint \frac{\partial \varphi}{\partial n_1}\left(\frac{1}{4\pi r}\right) d\Sigma$$

$$+ \iint \varphi \frac{\partial}{\partial n_1}\left(\frac{1}{4\pi r}\right) d\Sigma + \frac{\varphi(P_*)}{2}$$

After combining terms, the form of Eq. A.1 on the body surface is given as

$$\varphi = -\iint \frac{\partial \varphi}{\partial n_1} \frac{1}{2\pi r}\, d\Sigma \; + \qquad \text{A.11}$$

$$\iint \varphi \frac{\partial}{\partial n}\left(\frac{1}{2\pi r}\right) d\Sigma$$

where the second integral is obtained as a limiting case for $\varepsilon \to 0$.

APPENDIX B

WAKE FORMULATION

For completeness, the formulation of the wake given in Ref. 3 is summarized here. According to the linearized Bernoulli Equation, Eq. 1.15, for steady flow, there can be no pressure jump through the wake so that on the wake

$$\frac{\partial}{\partial x_1}\left(\varphi_u - \varphi_\ell\right) = 0 \qquad \text{B.1}$$

For Eq. 1.15, the expression for I_W is written as

$$I_W = \iint_{\Sigma_W} \left(\varphi_u - \varphi_\ell\right) \frac{\partial}{\partial n}\left(\frac{1}{r}\right) d\Sigma \qquad \text{B.2}$$

where Σ_W is the upper surface of the wake and n_1 is understood to be the upper normal. The surface Σ_W is shown in Fig. B1. Note that the surface of the wake is not known and Eq. 1.14, which is satisfied on the body, must be completed by the equation on the wake. From Eq. 1.15, the velocity on the wake is tangent to the surface of the wake. What results is two coupled equations, one on the body with $\partial\varphi/\partial n$ known and φ unknown and the second on the wake with $\partial\varphi/\partial n$ unknown and $\Delta\varphi\,(=\varphi_u - \varphi_\ell)$ constant along the x - direction on the wake and

equal to the value of $\Delta\varphi$ at the trailing edge. The geometry of the wake is determined given the condition that the velocity is tangent to the wake by knowing the velocity on the wake, $\partial\varphi/\partial n$.

To simplify the above procedure, consider the following. First note that

$$\iint \frac{\partial}{\partial n_1}\left(\frac{1}{r}\right) d\Sigma = -\iint \frac{\bar{n}_1 \cdot \bar{r}}{r^3}\, d\Sigma$$

$$= -\iint \bar{n}_1 \cdot \frac{\bar{r}}{r}\, \frac{d\Sigma}{r^2} \qquad \text{B.3}$$

$$= -\iint \frac{d\Sigma_n}{r^2}$$

$$= -\iint d\Omega$$

where

$$d\Sigma_n = \bar{n}_1 \cdot \frac{\bar{r}}{r} d\Sigma = d\Sigma \cos(n,r)$$

and $d\Omega$ is the solid angle shown in Fig. 26 as

$$d\Omega = \frac{d\Sigma_n}{r^2} \qquad \text{B.4}$$

Next, consider the wake integral as a sum of strips of width dy in the x direction as shown in Fig. B2. Applying the mean value theorem to Eq. B.2 combined with B.3 yields

$$I_w = -\iint_{\Sigma_w} \Delta\varphi(y)\, d\Omega$$

$$= -\sum_j \Delta\Phi(y_j) \iint_{\Sigma_j} d\Omega \qquad \text{B.5}$$

By noting that the integral is the solid angle Ω_j for each element Σ_j one obtains

$$I_w = -\sum \Delta\varphi(y_j)\, \Delta\Omega_j \qquad \text{B.6}$$

(Note that $\Delta\varphi$ is a function of y only)

From Eq. B.6, it can be seen that the wake contribution is a function of the solid angle so that a reasonable geometry for the

wake is one in which the solid angles $\Delta\Omega_j$ remain fairly constant. This suggests the possibility of approximating the wake by straight vortex lines, parallel to the direction of flow, emanating from the trailing edge of the wing since geometrical considerations show that the solid angles change only slightly[3]. With this assumption, the wake equation simplifies considerably and its contribution reduces to a line integral. Assuming the trailing edge to be given by

$$X = X_{TE}(Y)$$

$$Z = Z_{TE}(Y)$$

the equation of the wake surface becomes

$$S_w = Z_1 - Z_{TE}(Y) = 0$$

and

$$I_w = -\iint \Delta\varphi (\bar{\nabla} S \cdot \bar{r}) \frac{1}{r^3} \, dx_1 dy_1$$

$$= -\iint \Delta\varphi \left[-\frac{dZ_{TE}}{dY_1}(Y_1 - Y) + Z_w(Y_1) - Z \right] \frac{dx_1 dy_1}{r^3} \qquad 8.7$$

$$= \int_{-b/2}^{+b/2} \Delta\varphi \, J_w \, dy_1$$

where b is the span of the wing and

$$J_w = \left[Z_1 - Z - \frac{dZ_{TE}}{dY}(Y_1 - Y) \right] \int_{X_{TE}}^{\infty} \frac{1}{r^3} dX_1$$

$$= \left[(Z_1 - Z) - \frac{dZ_{TE}}{dY}(Y_1 - Y) \right] \frac{-1}{(Y-Y_1)^2 + (Z-Z_1)^2} \left[\frac{X_1 - X}{r} \right]_{X_{TE}}^{\infty} \qquad \text{B.8}$$

with $Z_1 = Z_W(Y)$. If the trailing edge is in the plane $Z_1 = 0$, Eq. B.8 reduces to

$$J_w = \frac{+Z}{(Y_1 - Y)^2 + Z^2} \left[1 - \frac{X_{TE} - X}{\left\{ (X_{TE} - X)^2 + (Y_1 - Y)^2 + Z^2 \right\}^{1/2}} \right]$$

Note that the above discussion is for bodies with a sharp trailing edge only as it depends upon the known location of the stagnation point from which the wake emanates. For bodies without a sharp edge, e.g., a rotating cylinder, this formulation is not applicable.

APPENDIX C

As mentioned in Subsection 5.2, the coefficients

$$C_{ki} = \iint_{\Sigma_i} \frac{\partial}{\partial n_1} \left(\frac{1}{2\pi R_k} \right) d\Sigma_i \qquad \text{C.1}$$

are evaluated by approximating the surface element Σ_i with its tangent plane at the centroid of the element. This value can eventually be corrected by adding the integral of the difference between the original integrand and the (tangent-element) approximate integrand. This integral can be evaluated numerically by using standard Gaussian quadrature formulas. However, in the case of k = i (effect of the element on itself) the tangent plane contribution is equal to zero. Furthermore, the integrand becomes infinite when $R_k = 0$. Hence, a special integration scheme must be used. In this appendix an analysis of the type of singularity of the integrand of Eq. C.1 (when k = i) is given. Then a transformation that eliminates the singularity is presented.

First consider the behavior of the doublets in the neighbornood of the singularity. For simplicity, the analysis of the behavior of the doublet in the neighborhood R = 0 is performed with a frame of reference such that origin is at the centroid of the element and the z axis is directed as the normal n. Then the equation of the element can be

written as

$$Z - F(X,Y) = 0 \qquad \text{C.2}$$

with z = 0 for x = y = 0 (Fig. C.1) and Eq. C.1 for k = i reduces to

$$C_{KK} = -\iint_{\Sigma_K} \frac{h}{R^3}\, dx_1\, dy_1 \qquad \text{C.3}$$

where

$$h = -\frac{\partial F}{\partial X_1}(X_1 - X) - \frac{\partial F}{\partial Y_1}(Y_1 - Y) + (Z_1 - Z) \qquad \text{C.4}$$

is the distance along the normal $\bar{n}_1$ of the origin from the point x_1, y_1, z_1, (Fig. C.2). If R goes to zero the distance h goes also to zero. More precisely, as R goes to zero

$$h \approx Q R^2 \qquad \text{C.5}$$

where $Q = 1/\rho_c$ is the curvature of the cross section indicated in the figure (ρ_c is the radius of curvature). Thus, in a neighborhood of R = 0, Eq. C.3 reduces to

$$c_{kk} \approx -\iint \frac{Q}{R}\, dx_1\, dy_1 \qquad \text{C.6}$$

It should be noted that Q is the curvature of the cross section and thus Q depends upon the angle ψ of the cross section. Thus, in order to evaluate Eq. C.3, it is convenient to use polar coordinates since this eliminates the singularity as well as the sharp variations (in the plane, x_1, y_1) of the integrand due to the dependence of Q upon ψ .

Next consider the integration scheme. As shown above, the integration of Eq. C.1 (with k = i) in the neighborhood of the centroid of the elemenc can be performed using standard quadrature techniques (Gaussian quadrature in particular) in polar coordinates. However, the domain of integration is not simply defined with these variables. Hence, a more suitable technique (fully correspondent

to integration in polar coordinate) is described here.

As mentioned in Subsection 2.3, the boundary of the element in the plane are given by

$$\bar{X}_c - \Delta\bar{x} \leq \bar{x} \leq \bar{X}_c + \Delta\bar{X}$$

$$\bar{Y}_c - \Delta\bar{y} \leq \bar{y} \leq \bar{Y}_c + \Delta\bar{Y} \qquad \text{C.7}$$

Note that the use of $\bar{x}$, $\bar{y}$ variables

$$\xi = \bar{x}^2$$
$$\eta = \left[1 - (1 - \bar{y})^2\right] \frac{\bar{y}}{|\bar{y}|} \qquad \text{C.8}$$

has the advantage of eliminating the square root singularity at the leading edge and the tip*. On the other hand, a singularity of the type R^{-1} in the plane x_1, y_1 yields a singularity of the type $\bar{R}^{-1}$ in the plane $\bar{x}$, $\bar{y}$. Thus the integral to be evaluated is of the type

$$C_{KK} = \iint_D \frac{f(\bar{X},\bar{Y})}{\sqrt{\bar{X}^2+\bar{Y}^2}}\, d\bar{X}\, d\bar{Y}$$
$$= \int_{\bar{Y}_c-\frac{1}{2}\Delta\bar{Y}}^{\bar{Y}_c+\frac{1}{2}\Delta\bar{Y}} d\bar{Y} \int_{\bar{X}_c-\frac{1}{2}\Delta\bar{X}}^{\bar{X}_c+\frac{1}{2}\Delta\bar{X}} \frac{f(\bar{X},\bar{Y})}{\sqrt{\bar{X}^2+\bar{Y}^2}}\, d\bar{X} \qquad \text{C.9}$$

*This singularity is due to the factor $|\nabla s|$ in $d\Sigma = \left|\frac{\nabla s}{\partial s/\partial z}\right| dx_1 dy_1$

where $f(\bar{x}, \bar{y})$ is a finite but discontinuous function of $\bar{x}$ and $\bar{y}$ (the discontinuity being due to the "cross-section-curvature effect") but continuous in polar coordinates.

In order to analyze Eq. C.7, it is convenient to separate the contributions of $D_1 + D_3$ and $D_2 + D_4$ (Fig. C.3) as

$$C_{KK} = C'_{KK} + C''_{KK} \qquad \text{C.10}$$

with

$$C'_{KK} = \iint_{D_1 + D_3} f(\bar{x}, \bar{y})\, d\bar{x}\, d\bar{y} \qquad \text{C.11}$$

and

$$C''_{KK} = \iint_{D_2 + D_4} f(\bar{x}, \bar{y})\, d\bar{x} d\bar{y} \qquad \text{C.12}$$

Using the transformation

$$\begin{aligned} \bar{x} &= \bar{x}_c + \frac{\Delta\bar{x}}{2} u \qquad -1 \le u \le +1 \\ \bar{y} &= \bar{y}_c + \frac{\Delta\bar{y}}{2} v u \qquad -1 \le v \le +1 \end{aligned} \qquad \text{C.13}$$

Equation C.11 reduces to

$$c_{KK} = \frac{\Delta X \Delta Y}{A} \int_{-1}^{+1}\int_{-1}^{+1} f(u,v)|u|\,du\,dv \qquad C.14$$

Note that f(u, v)|u is a regular function of u and v since the factor u compensates for the $(\bar{x}^2 + \bar{y}^2)^{-1/2}$ singularity and the "cross-section-curvature effect" disappears in the u, v plane (which is similar to polar coordinate plane). Hence, Eq. C.14 can be evaluated by Gaussian quadrature. A similar transformation can be used in Eq. C.12.

This procedure was used to evaluate not only the effect c_{kk} of the element on itself but also for the effect of an element on the opposite element (e.g., leading edge root boxes on opposite surfaces). A similar technique is also used for the evaluation of

$$b_K = \sum b_{Ki}$$

$$= \sum_{i=1}^{N} \iint_{\Sigma_i} \Phi_i \frac{1}{R_K}\, d\Sigma_K$$

APPENDIX D

MODAL METHOD DERIVATIONS

This Appendix gives the derivations of the mode shapes for the symmetrical and anti-symmetrical modes and the expression for the pressure coefficient. First, consider the symmetrical modes as given by

$$\varphi^S = \sum \phi^S_{mn} U^S_n(x) V^S_m(y) \qquad \text{D.1}$$

From Fig. 6A, the symmetric components of the potential can be approximated in the chordwise direction by

$$U^S_n(x) = x^n \qquad n = 0, 1, 2, \ldots \qquad \text{D.2}$$

and the spanwise direction by

$$V^S_m(y) = y^{2m} \qquad m = 0, 1, 2, \ldots \qquad \text{D.3}$$

Next to be considered is the anti-symmetrical modes as shown in Fig. 6B. Here not only the shape of the potential, but also the shape of its derivative which has the form of the well known pressure distribution curve must also be derived. Note that the curve is infinite at the leading edge and drops to zero as the square root of x, the distance

from the trailing edge. Consequently, a function satisfying all these conditions is necessary. A function such as this is classically given by

$$C_p = -2\varphi_x$$

$$= \pm\sqrt{\frac{1-x}{x}}\sum C_n(y)(1-x)^n \qquad \text{D.4}$$

where φ_x represents the derivative of C_p with respect to x. Examination of Eq. D.4 shows that it gives the required conditions at the leading edge, where x = 0, and is singular (i.e., $C_p = \infty$) and also that as x approaches 1, near the trailing edge, it behaves as the square root of the distance from the trailing edge, 1-x. Since Eq. D.4 satisfies all the necessary conditions, it can be integrated to obtain φ or

$$\varphi = \pm\left(\frac{1}{2}\right)\int_0^c \left[\sqrt{\frac{1-x}{x}}\sum_0^M C_m(1-x)^m\right]dx_1 \qquad \text{D.5}$$

where the limits are from the leading edge to the trailing edge, c. Integration of this equation is shown in the following:

$$I = \sqrt{\frac{1-X}{X}} \sum C_m (1-X)^m$$

$$= \sum_{m=0}^{N} \left[\phi_{m+1} \left(m + \tfrac{3}{2} \right) - \phi_m \right] \sqrt{\frac{1-X}{X}} \, (1-X)^m \qquad \text{D.6}$$

where

$$C_m = \phi_{m+1} \left(m + \tfrac{3}{2} \right) - m \phi_m$$

with

$$\phi_{N+1} \equiv 0$$

which becomes

$$I = \sum_{m=0}^{N-1} \phi_{m+1} \sqrt{\frac{1-X}{X}} \, (1-X)^m \left(m + \tfrac{3}{2} \right) - \sum_{m=0}^{N} \phi_m \sqrt{\frac{1-X}{X}} \, (1-X)^m \qquad \text{D.7}$$

with $\phi_{n+1} \equiv 0$. Next

$$I = \sum_{n=1}^{N} \phi_n \sqrt{\frac{1-x}{x}} (1-x)^{n-1} \left(n + \tfrac{1}{2}\right)$$

$$- \phi_o \left(\tfrac{1}{2}\right) \frac{1}{\sqrt{x(1-x)}} - \sum_{n=o}^{N} \phi_n \sqrt{\frac{1-x}{x}} (1-x)^n \qquad \text{D.8}$$

where n = m + 1. Combining the first and third terms yields

$$I = \sum_{o}^{N} \phi_n \sqrt{\frac{1-x}{x}} (1-x)^{n-1} \left[\left(n + \tfrac{1}{2}\right) - (1-x)\right] - \phi_o \left(\tfrac{1}{2}\right) \frac{1}{\sqrt{x(1-x)}} \qquad \text{D.9}$$

Next, integrating

$$\varphi = \pm \int I \, dx = \pm \left[\sum_{o}^{N} \phi_n \sqrt{x(1-x)} (1-x)^n - \phi_o \, \mathrm{Tan}^{-1} \sqrt{\frac{x}{1-x}} \right] \qquad \text{D.10}$$

Finally, consider the formulation for the pressure distribution. From Eq. 1.11, the expression relating C_p with the potential involves a derivative with respect to x, the direction of the flow. From this relation, it is seen that the expression for the modes is an analytical differentiation with respect to x.

Begin by considering the symmetric component of the potential in the chordwise direction only. From Section 3 this is given by

$$U_n^S(x) = x^n$$

The pressure coefficient mode shape resulting from this component is given by

$$\frac{\partial}{\partial x}\left[U_n^S(x)\right] = \frac{\partial}{\partial x}(\varphi)$$

or

$$\frac{\partial}{\partial x}\left[U_n^S(x)\right] = nx^{n-1} \qquad \text{D.11}$$

Next, the anti-symmetric component is considered. Care must be taken as the arc-tangent term is considered only n = 0, the first mode. The upper-surface component is given as

$$\varphi = \sum_{n=0}^{N} \left(\phi_n \sqrt{x(1-x)}\ (1-x)^n \right)$$

$$- \phi_o \operatorname{Tan}^{-1} \sqrt{\frac{x}{1-x}} \qquad \text{D.12}$$

First, consider the evaluation of pressure coefficient. Eq. 1.11, for the kth mode, U_k, Eq. D.12.

$$U_k' = \tfrac{1}{2} x^{-\frac{1}{2}} (1-x)^{k-\frac{1}{2}}$$

$$+ \sqrt{x}\ (1-x)^{k-\frac{3}{2}} (k-\tfrac{1}{2})(-1) \qquad \text{D.13}$$

which becomes

$$u_k' = \frac{1}{2}\sqrt{\frac{1-x}{x}}\left[(1-x)^{k-1} - (1-x)^{k-2}(2)\left(k-\frac{1}{2}\right)\right]$$

and finally

$$u_k' = \frac{1}{2}\sqrt{\frac{1-x}{x}}(1-x)^{k-2}\left[(1-x) - (2k-1)\right] \qquad \text{D.14}$$

It should be noted that an arc-tangent term appears in the first mode (see Eq. D.12). Differentiating the first mode yields

$$u_1' = \frac{1}{2}\sqrt{\frac{1-x}{x}}(1-x)^{-1}\left[(1-x)-1\right] + \frac{1}{2}\frac{1}{\sqrt{x(1-x)}} \qquad \text{D. 15}$$

Note that the last term contains the arc-tangent contribution. Combining terms gives

$$u_1' = \left(\frac{1}{2}\right)\frac{1}{\sqrt{x(1-x)}}\left[(1-x)\right.$$

$$\left. -1 \quad +1 \right]$$

or

$$u_1' = \frac{1}{2}\sqrt{\frac{1-x}{x}} \qquad \text{D.16}$$

Equations D.14 and D.12 give the relations for the pressure coefficient for the first through Kth modes.

FIGURES

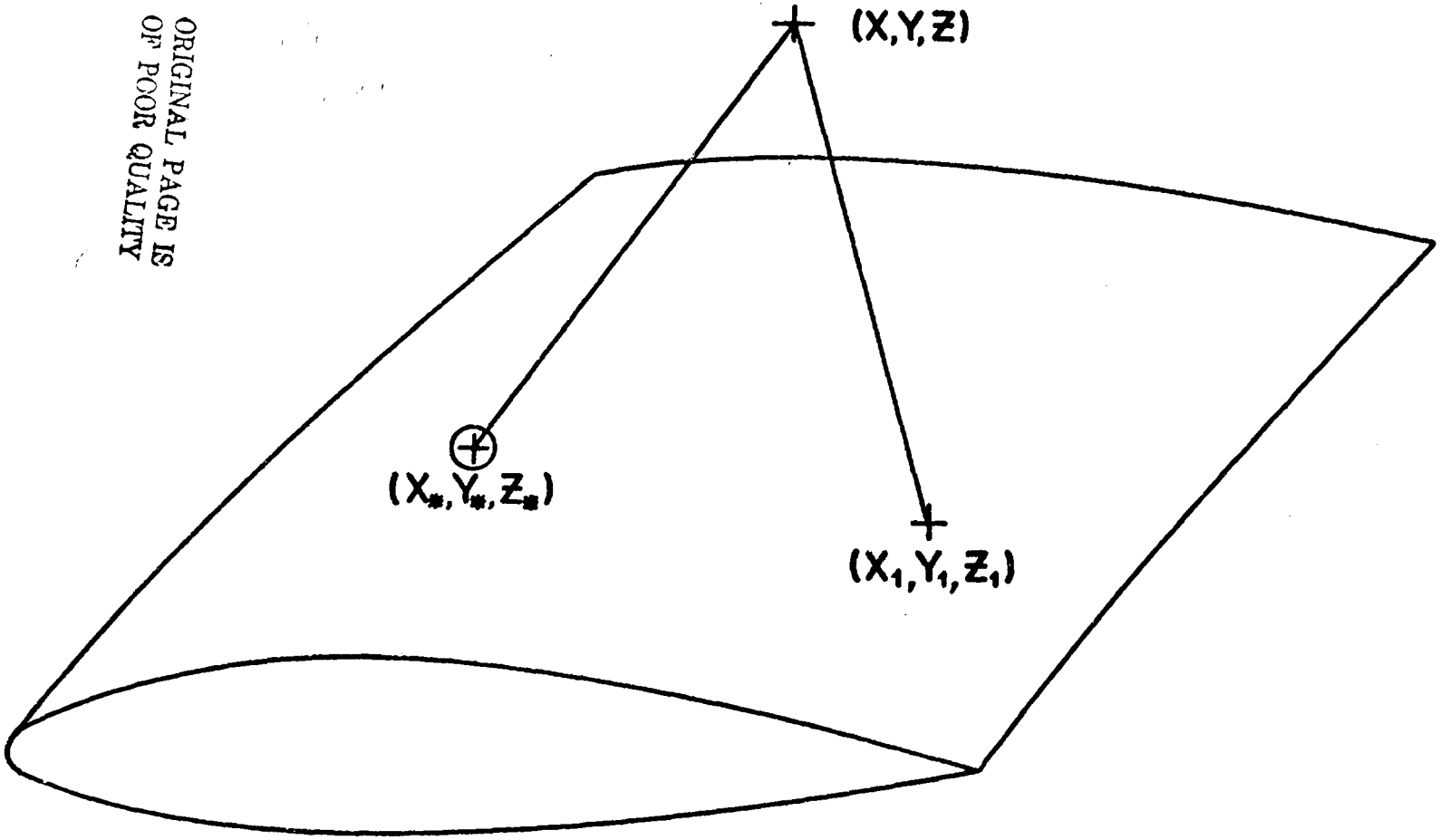

EVALUATION AND INFLUENCE POINTS
FIGURE A1

LOCAL COORDINATE SYSTEM
FIGURE A2

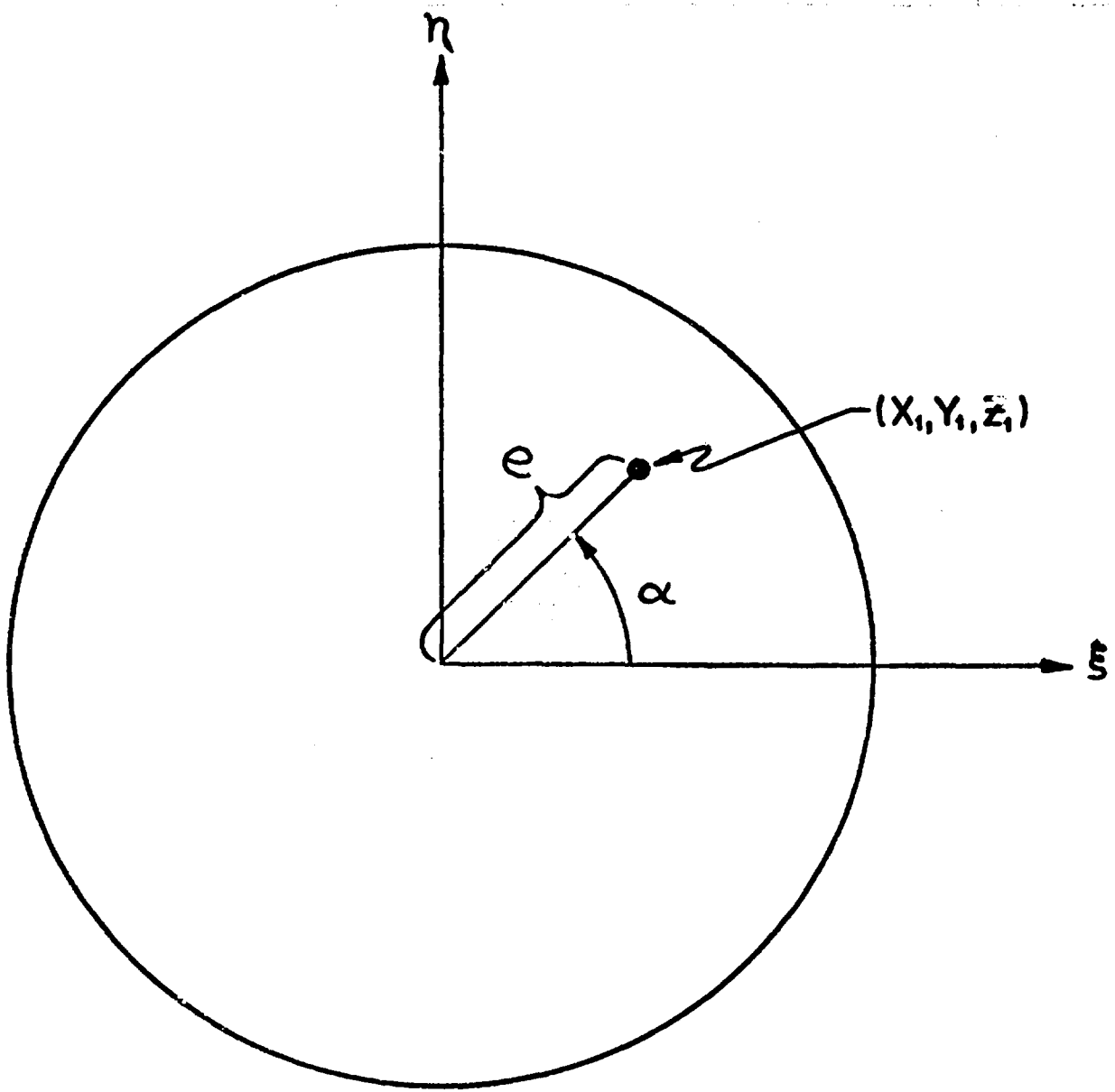

TANGENT PLANE σ

FIGURE A3

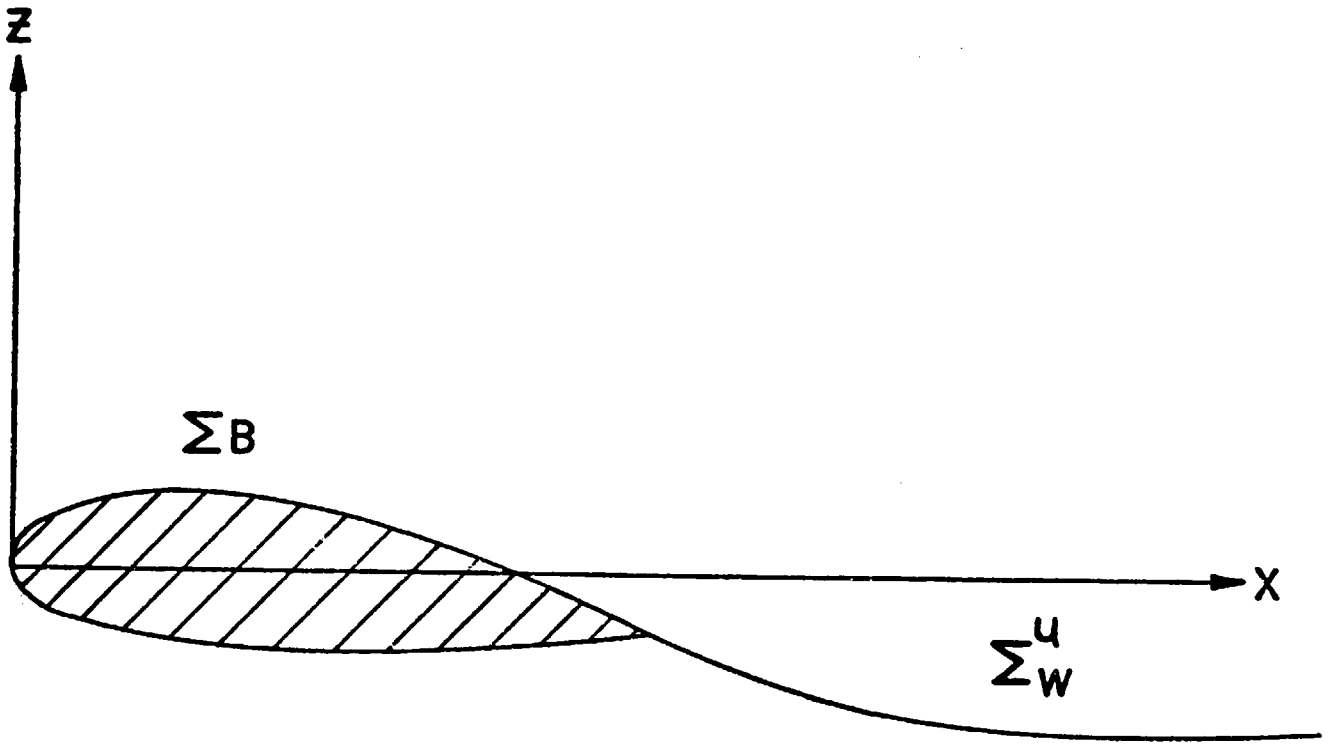

WAKE GEOMETRY
FIGURE B1

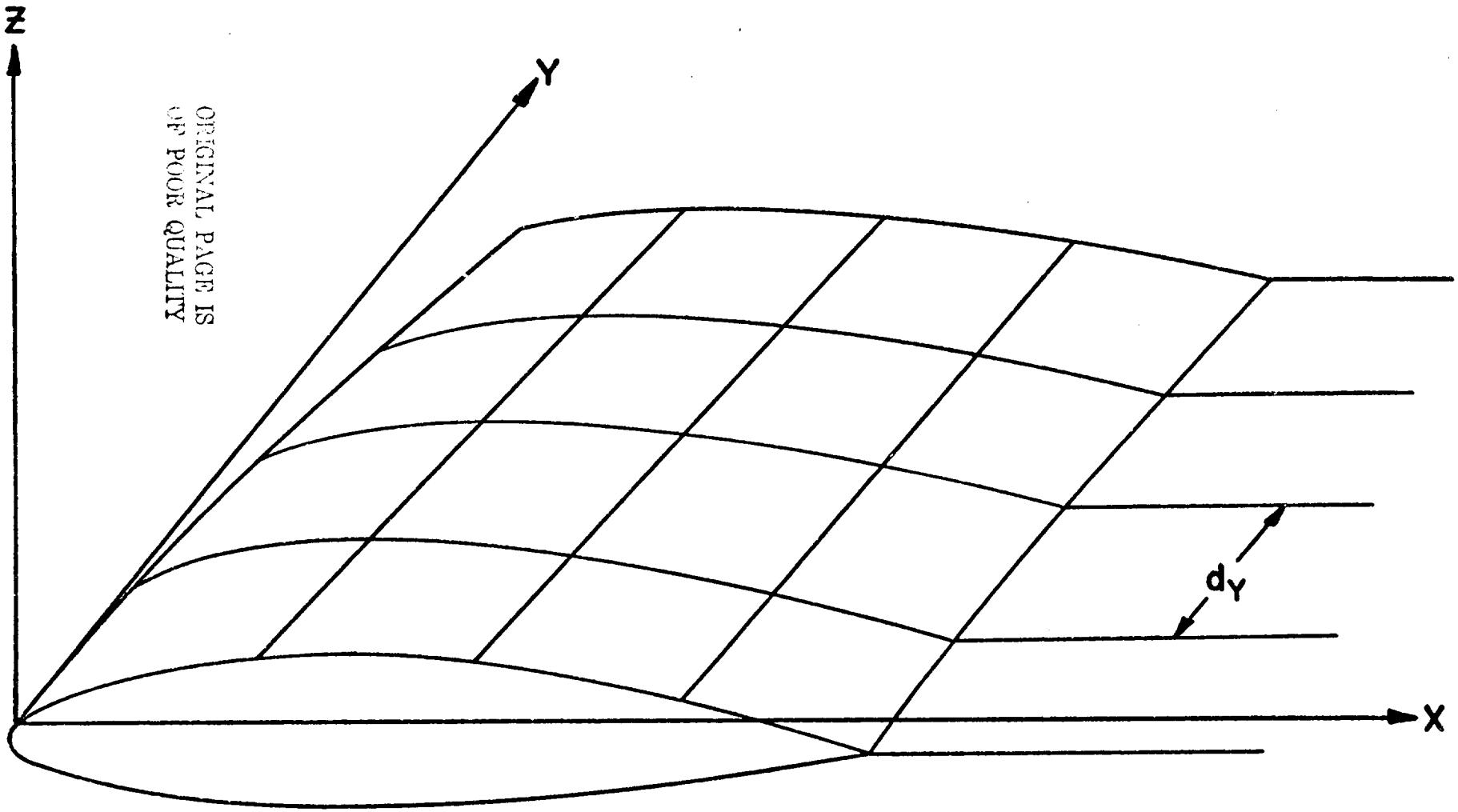

WAKE EVALUATION
FIGURE B2

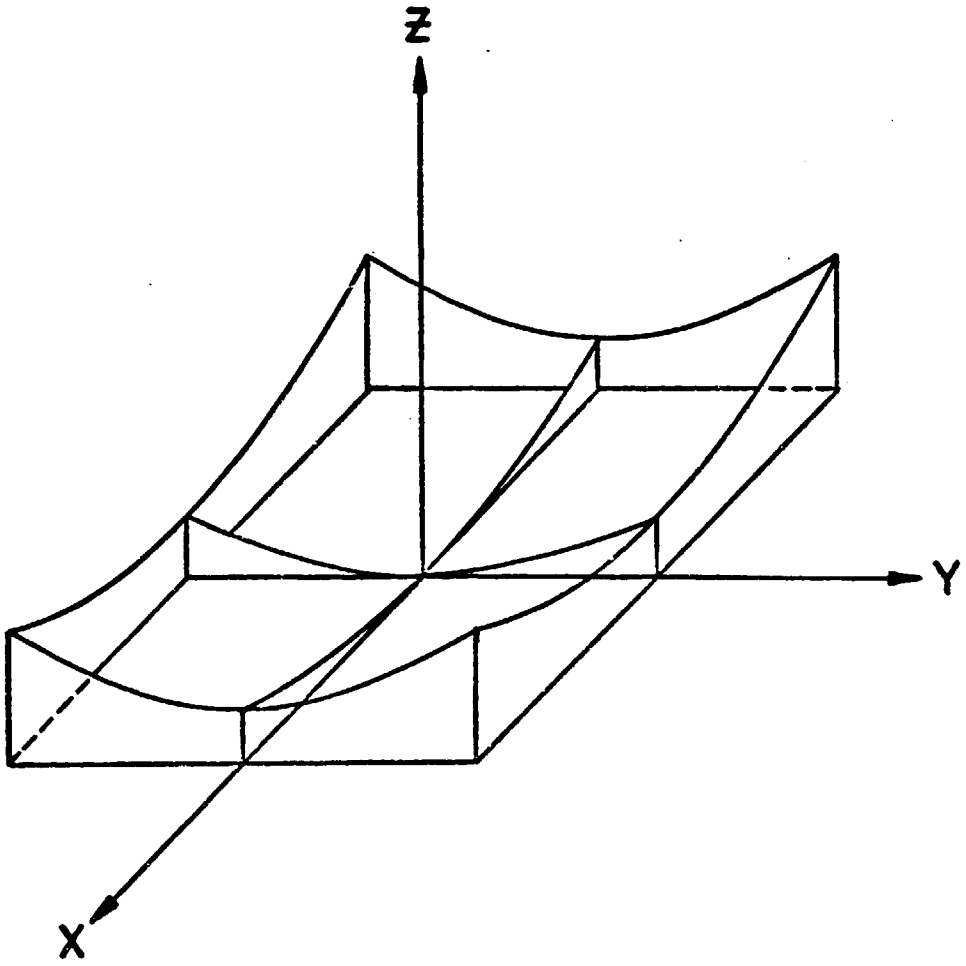

DOUBLET BEHAVIOR IN THE AREA OF THE SINGULARITY

FIGURE C1

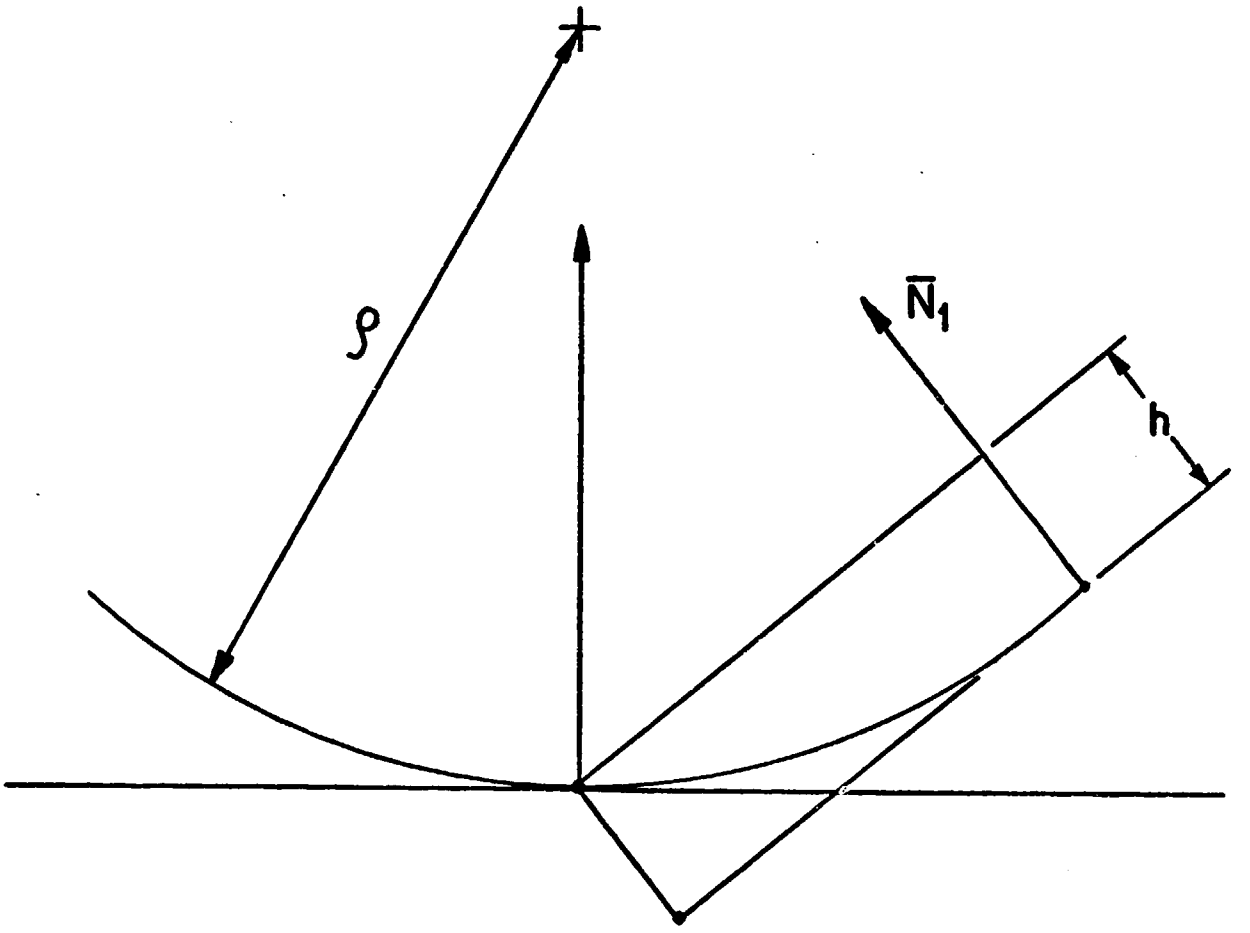

RADIUS OF CURVATURE
FIGURE C2

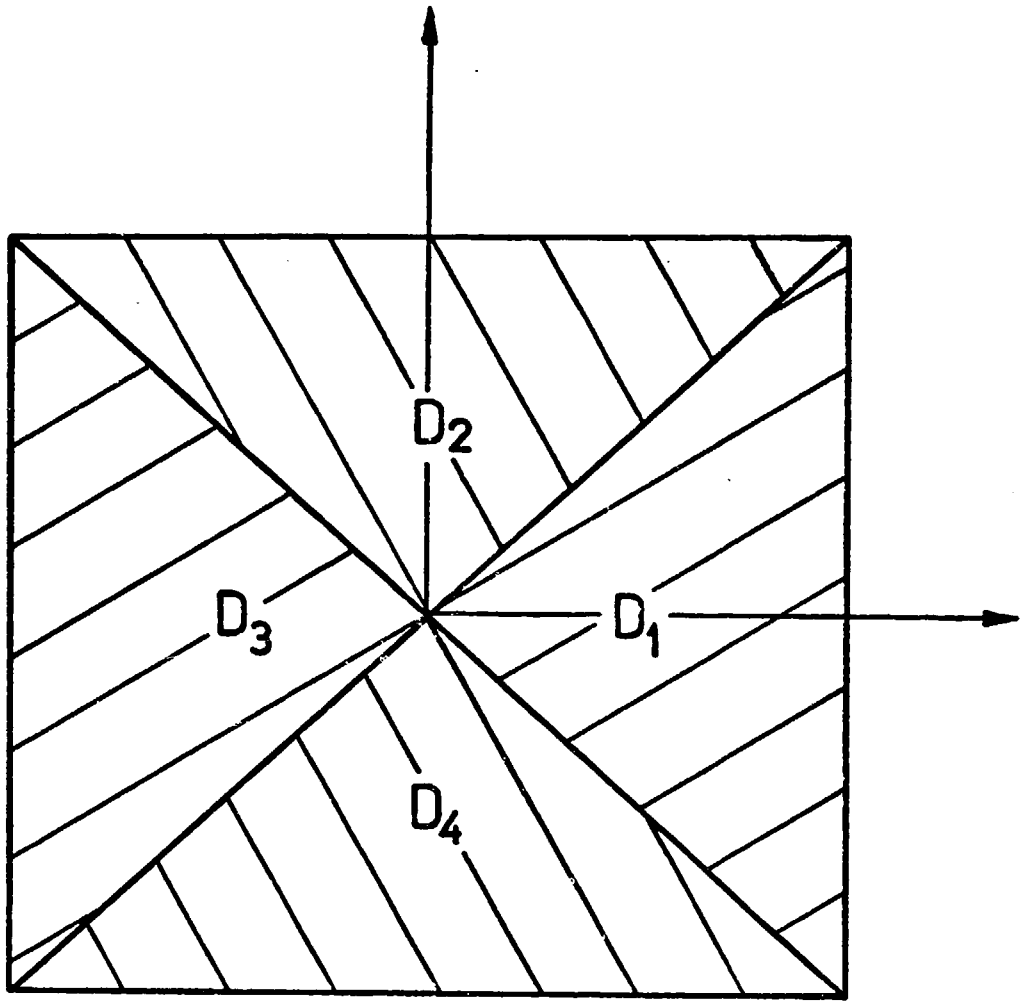

INTEGRATION SCHEME
FIGURE C3